

ACOUSTIC LOAD ON A PLATE WITH APPLICATION TO WATER-BORNE TSUNAMI DEBRIS

A THESIS SUBMITTED TO THE GRADUATE DIVISION OF THE  
UNIVERSITY OF HAWAI'I AT MĀNOA IN PARTIAL FULFILLMENT  
OF THE REQUIREMENTS FOR THE DEGREE OF

MASTER OF SCIENCE

IN

MECHANICAL ENGINEERING

MAY 2023

By

Edward A. Vause

Thesis Committee:

Marcelo Kobayashi, Chairperson

John Allen

H. Ronald Riggs

## **Acknowledgements**

The author would like to acknowledge the assistance of the committee, especially during the last few weeks of the preparation of the manuscript during which some members were extremely busy. In particular, the author would like to express tremendous gratitude to Professor John Allen, who joined the committee about two weeks before the defense of this thesis. The author would also like to express gratitude to Professor A. Zachary Trimble who was for a while on the committee, but did not end up serving during the defense and preparation of the final manuscript. The author nonetheless found discussions with him to be very illuminating.

The author would like to thank his family and friends for their support during his journey to completing this research. In particular, without the support of his parents, this work likely would not have made it to completion.

## **Abstract**

Water-borne debris carried by the strong flow of water of a tsunami, flood, or storm surge can damage structures in the inundation zone. A prominent example of such debris is a shipping container. Research on such debris has focused on the impact between the debris and the structure. This work instead focuses on the effect of the water on the debris once the debris has made contact with a structure. A 2-dimensional analytical model of the draft (submerged) portion of the water-impacted panel of a shipping container is presented. The water carrying the shipping container is modeled as an acoustic load, which provides a conservative upper bound of the pressure of the water on the container. The draft portion of the water-impacted face of the shipping container is modeled as a Kirchhoff-Love plate, which describes the elastic deformation of this portion of the container. The model is validated using finite element models for the six cases of a 20-foot and 40-foot shipping container, each at 100%, 50%, or zero cargo capacity. The results indicate that varying the mass of the cargo in the shipping container yields no significant difference in the deformation. The acoustic load is by far the most significant at the bottom of the container, whereas the rest of the water-impacted panel experiences steady displacement, continuing with the constant velocity of the water. Most of the deformation of the important bottom region occurs within the acoustic time scale of the water.

# Table of Contents

<b>Acknowledgements</b> . . . . .	<b>ii</b>
<b>Abstract</b> . . . . .	<b>iii</b>
<b>List of Tables</b> . . . . .	<b>vi</b>
<b>List of Figures</b> . . . . .	<b>vii</b>
<b>Chapter 1: Introduction</b> . . . . .	<b>1</b>
1.1 Context . . . . .	1
1.2 Literature Review . . . . .	1
1.3 Description of the Problem . . . . .	2
<b>Chapter 2: Analytical Model</b> . . . . .	<b>4</b>
2.1 Formulation . . . . .	4
2.1.1 Acoustic Load . . . . .	4
2.1.2 Dimensional Model . . . . .	5
2.1.3 Nondimensionalized Model . . . . .	8
2.2 Analytical Solution . . . . .	9
<b>Chapter 3: Numerical Validation</b> . . . . .	<b>14</b>
3.1 The Draft-Portion Model (DPM) . . . . .	14
3.2 The Full-Plate Model (FPM) . . . . .	14
3.3 Description of the Finite Element Models . . . . .	15
<b>Chapter 4: Results</b> . . . . .	<b>18</b>
4.1 Stiffnesses of the Bottom and Top of the Shipping Container . . . . .	18
4.2 Results from the Models . . . . .	19
4.3 20-Foot Container at 100% Capacity . . . . .	21
4.4 20-Foot Container at 50% Capacity . . . . .	26
4.5 20-Foot Container Empty . . . . .	31
4.6 40-Foot Container at 100% Capacity . . . . .	36

4.7	40-Foot Container at 50% Capacity . . . . .	41
4.8	40-Foot Container Empty . . . . .	46
4.9	Discussion of the Results . . . . .	51
	<b>Chapter 5: Conclusions and Future Work . . . . .</b>	<b>53</b>
5.1	Conclusions . . . . .	53
5.2	Future Work . . . . .	53
	<b>References . . . . .</b>	<b>55</b>

## List of Tables

4.1	20', 100%: analytical results. . . . .	21
4.2	20', 50%: analytical results. . . . .	26
4.3	20', empty: analytical results. . . . .	31
4.4	40', 100%: analytical results. . . . .	36
4.5	40', 50%: analytical results. . . . .	41
4.6	40', empty: analytical results. . . . .	46

## List of Figures

1.1	Water-borne shipping container impact on a structure. . . . .	2
2.1	Draft portion of the water-impacted panel. . . . .	7
3.1	The draft-portion model within the full-plate model. . . . .	15
4.3.1	20', 100%: displacement comparisons of finite element DPM and FPM. . . . .	21
4.3.2	20', 100%: comparison of analytical model and DPM at $z = 0$ . . . . .	21
4.3.3	20', 100%: $z = 0$ , displacement vs. logarithm of time. . . . .	22
4.3.4	20', 100%: comparison of analytical model and DPM at $z = 1/2$ . . . . .	22
4.3.5	20', 100%: comparison of analytical model and DPM at $z = 1$ . . . . .	22
4.3.6	20', 100%: analytical 2-D displacement of the draft portion of the plate. . . . .	23
4.3.7	20', 100%: FPM 2-D displacement of the full plate. . . . .	24
4.3.8	20', 100%: relative acoustic load over the plate. . . . .	25
4.4.1	20', 50%: displacement comparisons of finite element DPM and FPM. . . . .	26
4.4.2	20', 50%: comparison of analytical model and DPM at $z = 0$ . . . . .	26
4.4.3	20', 50%: $z = 0$ , displacement vs. logarithm of time. . . . .	27
4.4.4	20', 50%: comparison of analytical model and DPM at $z = 1/2$ . . . . .	27
4.4.5	20', 50%: comparison of analytical model and DPM at $z = 1$ . . . . .	27
4.4.6	20', 50%: analytical 2-D displacement of the draft portion of the plate. . . . .	28
4.4.7	20', 50%: FPM 2-D displacement of the full plate. . . . .	29
4.4.8	20', 50%: relative acoustic load over the plate. . . . .	30
4.5.1	20', empty: displacement comparisons of finite element DPM and FPM. . . . .	31
4.5.2	20', empty: comparison of analytical model and DPM at $z = 0$ . . . . .	31
4.5.3	20', empty: $z = 0$ , displacement vs. logarithm of time. . . . .	32
4.5.4	20', empty: comparison of analytical model and DPM at $z = 1/2$ . . . . .	32
4.5.5	20', empty: comparison of analytical model and DPM at $z = 1$ . . . . .	32
4.5.6	20', empty: analytical 2-D displacement of the draft portion of the plate. . . . .	33
4.5.7	20', empty: FPM 2-D displacement of the full plate. . . . .	34
4.5.8	20', empty: relative acoustic load over the plate. . . . .	35
4.6.1	40', 100%: displacement comparisons of finite element DPM and FPM. . . . .	36
4.6.2	40', 100%: comparison of analytical model and DPM at $z = 0$ . . . . .	36

4.6.3 40', 100%: $z = 0$ , displacement vs. logarithm of time. . . . .	37
4.6.4 40', 100%: comparison of analytical model and DPM at $z = 1/2$ . . . . .	37
4.6.5 40', 100%: comparison of analytical model and DPM at $z = 1$ . . . . .	37
4.6.6 40', 100%: analytical 2-D displacement of the draft portion of the plate. . . . .	38
4.6.7 40', 100%: FPM 2-D displacement of the full plate. . . . .	39
4.6.8 40', 100%: relative acoustic load over the plate. . . . .	40
4.7.1 40', 50%: displacement comparisons of finite element DPM and FPM. . . . .	41
4.7.2 40', 50%: comparison of analytical model and DPM at $z = 0$ . . . . .	41
4.7.3 40', 50%: $z = 0$ , displacement vs. logarithm of time. . . . .	42
4.7.4 40', 50%: comparison of analytical model and DPM at $z = 1/2$ . . . . .	42
4.7.5 40', 50%: comparison of analytical model and DPM at $z = 1$ . . . . .	42
4.7.6 40', 50%: analytical 2-D displacement of the draft portion of the plate. . . . .	43
4.7.7 40', 50%: FPM 2-D displacement of the full plate. . . . .	44
4.7.8 40', 50%: relative acoustic load over the plate. . . . .	45
4.8.1 40', empty: displacement comparisons of finite element DPM and FPM. . . . .	46
4.8.2 40', empty: comparison of analytical model and DPM at $z = 0$ . . . . .	46
4.8.3 40', empty: $z = 0$ , displacement vs. logarithm of time. . . . .	47
4.8.4 40', empty: comparison of analytical model and DPM at $z = 1/2$ . . . . .	47
4.8.5 40', empty: comparison of analytical model and DPM at $z = 1$ . . . . .	47
4.8.6 40', empty: analytical 2-D displacement of the draft portion of the plate. . . . .	48
4.8.7 40', empty: FPM 2-D displacement of the full plate. . . . .	49
4.8.8 40', empty: relative acoustic load over the plate. . . . .	50

# Chapter 1

## Introduction

### 1.1. Context

Water-borne debris carried by the strong flow of water of a tsunami, flood, or storm surge can cause significant damage by impacting on structures in the inundation zone [16]. Understanding the effect of these impact forces on structures is crucial toward devising building codes that ensure that structures are resilient to such impacts. However, for sufficiently large debris that exhibit elastic behavior, understanding impact forces on the debris themselves may be important for accurately estimating the impact forces on the structure that is impacted by the debris. Such forces will be propagated through the debris to the structure. A shipping container carried by flowing water in an inundation zone is an example of a large piece of such debris, the elastic behaviour of which is the focus of this research.

### 1.2. Literature Review

Related research on inundation zone impacts has focused mostly on the impact between the debris and a structure [1, 2, 3, 11], or direct water impact on a structure [17]. The overarching conclusions of these studies include that the mass of a shipping container's cargo (non-rigidly attached, nonstructural mass) does not significantly affect the peak impact force, and that the impact force can be modeled by simple equations, most notably that the force is roughly linearly proportional to the velocity of the debris. Experimental studies on the impulse and work-energy relationships note that it is difficult to determine the time period over which the impact force is applied (for impulse) and the stopping distance of the debris after impact (to relate work done on the structure with the kinetic energy of the debris).

Comparisons between experiments using real shipping containers in water versus in-air experiments suggest that the effect of the water flow beyond simply carrying the debris is insignificant. The studies in [12] present a one-dimensional analytical model that provides some conservative upper-bound estimates of debris impacts, along with a two-dimensional numerical model that suggests that when the two-dimensionality of the water, i.e., a free surface is considered, the peak impact force is relevant over an acoustic time scale, as opposed to a longer time scale of the gravity waves formed against the debris.

### 1.3. Description of the Problem

As stated above, most of the related research has focused on the impact between the debris and a structure. This research, in contrast, focuses on the elastic behavior of a piece of debris, a shipping container, due to the impact of the water. Specifically, the focus is on the panel of the shipping container opposite to that of the structural impact, starting at the time that the container has impacted the structure, which is assumed to be rigid. Fig. 1.1 outlines this panel of the shipping container in a dotted box. This panel is referred to as the water-impacted panel.

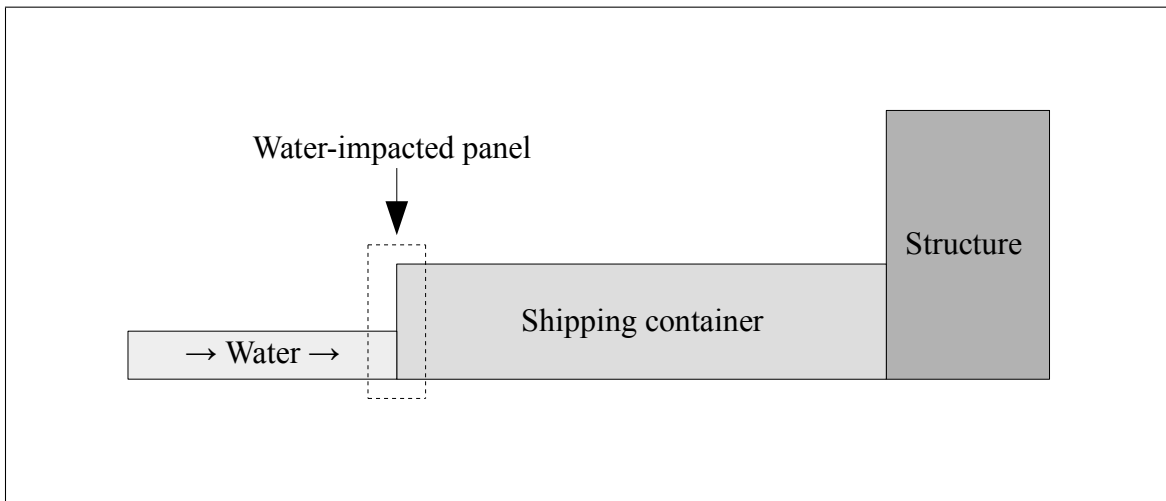


Figure 1.1: Water-borne shipping container impact on a structure.

Time begins at the time of impact of the shipping container on the structure. At this time, the water-impacted panel is moving at the same velocity as the water, so the water has not yet applied any load on this panel. After impact, the four panels (only the top and bottom of which are considered) and internal rails of the container to which the water-impacted panel is attached cause this panel to slow down, thus allowing the water to impact and apply a load on this panel. The portion of the water-impacted panel with which the water makes contact is referred to as the *draft portion*, the portion of the panel that is submerged.

The objective of this research is to derive and validate a preliminary analytical model of the draft portion of the water-impacted panel of the shipping container using Kirchhoff-Love plate theory and a simple acoustic load. This yields an elastic model of the behavior of a certain, common type of tsunami-driven debris, and the forces acting on it. Ultimately, the broader purpose of this and related studies

is to understand the forces on the debris-impacted structure. The force on the debris would propagate through the debris to the structure. This model, or an improved version of it, can thus contribute to further understanding of the forces structures impacted by waterborne debris, by providing insight into the deformation of the debris, the load acting on it, and the time scale over which the impact may be important.

# Chapter 2

## Analytical Model

### 2.1. Formulation

A classical Kirchhoff-Love rectangular plate with bending about only one axis is used to model the draft portion of the water-impacted panel of the shipping container. As opposed to beam theory, which involves the cross-sectional area of the beam, plate theory is expressed per unit width of the plate, and thus the solution applies to a plate of arbitrary width. The acoustic load that models the load due to the water is given by the pressure change across the pressure wave created by the impact of the water. The acoustic load is used as effective forcing and damping terms in the governing equation of the Kirchhoff-Love plate.

A dimensional model is presented, followed by a nondimensionalized model that is used to solve the problem. In the following sections, variables with a superscript asterisk (\*) denote dimensional variables that have nondimensional counterparts.

#### 2.1.1. Acoustic Load

The acoustic load that represents the load due to the water is modeled the same way as a transient pressure wave in a pipe. This theory can be found in studies of the phenomenon of a water hammer in water surge analysis in pipes, which models the pressure in a pipe when a valve is suddenly closed [18, 27]. At the time when the shipping container impacts the structure, the shipping container (or at least stiffer portions of it) will slow suddenly. At this time, if the water-impacted panel were rigid, it would act analogously to a valve suddenly stopping the flow of water. We assume initially that this panel is rigid.

The water in Fig. 1.1 is traveling to the right at a constant velocity  $u_0^*$  when the shipping container impacts the structure. Since the water impacts the shipping container, a pressure wave of relative velocity  $u_0^* - (-c_w) = u_0^* + c_w$ , where  $c_w$  is the speed of sound in water, with respect to the water flow is reflected off the water-impacted panel and travels upstream (to the left). However, since  $c_w$  is very large compared to  $u_0^*$ , this relative velocity can be approximated by  $c_w$ . The mass flow rate entering the wavefront is

$\rho_w u_0^* A_w$ , where  $\rho_w$  is the density of the water, and  $A_w$  is the cross-sectional area of the water flow, and thus the rate of change of momentum is approximately  $(\rho_w u_0^* A_w) c_w$  since the velocity of the water is zero at the water-impacted panel, assuming that the panel is rigid. Therefore, by Newton's second law, the force due to the water pressure,  $p$ , on the water-impacted panel is equal to the rate of change of momentum of the water, so

$$p A_w = (\rho_w u_0^* A_w) c_w, \quad (2.1)$$

and thus the pressure due to this acoustic load on a motionless (rigid) panel is

$$p = \rho_w c_w u_0^*, \quad (2.2)$$

which is known as the Joukowsky equation. However, since we consider the flexibility of the water-impacted panel in this model, the panel is not rigid, but rather experiences a displacement  $w^*(z^*, t^*)$  in the  $x^*$  direction (to the right) along its length in the  $z^*$  (vertical) direction with time  $t^*$ , and thus experiences a velocity of  $\frac{\partial w^*}{\partial t^*}$ . The velocity of the water at the panel is then  $\frac{\partial w^*}{\partial t^*}$  rather than zero, and thus Eq. 2.2 is instead,

$$p_{\text{rel}} = \rho_w c_w \left( u_0^* - \frac{\partial w^*}{\partial t^*} \right), \quad (2.3)$$

which represents the relative acoustic load, i.e., the pressure felt by the moving panel.

Before impact, the shipping container is carried by the water at a velocity of  $u_0^*$ . Therefore, since  $\frac{\partial w^*}{\partial t^*} = u_0^*$  instantaneously at the time of impact,  $p_{\text{rel}} = 0$  at this time. As the water-impacted panel slows down due to interaction with the adjacent panels of the shipping container to which it is attached, the pressure on the panel increases. Only if the panel were to come to a complete halt would the pressure on the panel be maximized to that given by Eq. 2.2. This simple acoustic load model provides a conservative upper bound of the pressure of the water on the container because it represents the maximum transient pressure due to the water and includes no free surface.

### 2.1.2. Dimensional Model

The governing equation of a Kirchhoff-Love plate subject to an acoustic load is

$$\rho_p h \frac{\partial^2 w^*(z^*, t^*)}{\partial t^{*2}} + D \frac{\partial^4 w^*(z^*, t^*)}{\partial z^{*4}} = p_{\text{rel}} = \rho_w c_w \left( u_0^* - \frac{\partial w^*(z^*, t^*)}{\partial t^*} \right), \quad (2.4)$$

or

$$\rho_p h \frac{\partial^2 w^*(z^*, t^*)}{\partial t^{*2}} + \rho_w c_w \left( \frac{\partial w^*(z^*, t^*)}{\partial t^*} - u_0^* \right) + D \frac{\partial^4 w^*(z^*, t^*)}{\partial z^{*4}} = 0, \quad (2.5)$$

in which:

$w^*(z^*, t^*)$  is the translational displacement in the  $x^*$  direction;

$z^*$  is the vertical direction, along the length of the plate;

$t^*$  is time;

$\rho_p$  is the density of the plate;

$h$  is the thickness of the plate in the  $x$  direction;

$\rho_w$  is the density of water;

$c_w$  is the speed of sound in water;

$u_0^*$  is the uniform initial velocity of the plate in the  $x^*$  direction;

$D = \frac{Eh^3}{12(1-\nu^2)}$  is flexural rigidity of the plate, where  $E$  and  $\nu$  are the Young's modulus and Poisson's ratio of the plate material, respectively.

This governing equation is similar to that of an Euler-Bernoulli beam in that displacement in only one dimension is considered. However, in Euler-Bernoulli theory, the flexural rigidity is  $EI$ , where the area moment of inertia  $I = h^4/12$ , instead of  $D$ . The factor of  $1 - \nu^2$  in plate theory corrects for the Poisson effect when a beam is wide enough to be considered a plate [30]. For a narrow beam experiencing bending, one side expands while the opposite side contracts due to the Poisson effect, a phenomenon known as anticlastic curvature. As the width of a beam approaches its length, i.e., as a beam becomes a plate, the additional material reduces the Poisson effect, increasing its flexural rigidity. Given that the water-impacted panel of the container has nearly square dimensions, this factor should be used, which, in the case of steel, the material of the container, significantly increases the rigidity of the plate compared to that in beam theory.

From Eq. 2.5, it can be seen that the plate under an acoustic load can be thought of as a plate experiencing viscous damping and a constant applied pressure, that is,

$$\rho_p h \frac{\partial^2 w^*(z^*, t^*)}{\partial t^{*2}} + \rho_w c_w \frac{\partial w^*(z^*, t^*)}{\partial t^*} + D \frac{\partial^4 w^*(z^*, t^*)}{\partial z^{*4}} = \rho_w c_w u_0^*. \quad (2.6)$$

Figure 2.1 illustrates the model of the draft portion of the plate. The translational spring  $k_1$  represents the stiffness of the bottom side of the shipping container, and its value is determined directly from the container's physical properties (see section 4.1). A fictitious translational spring  $k_2$  is added at

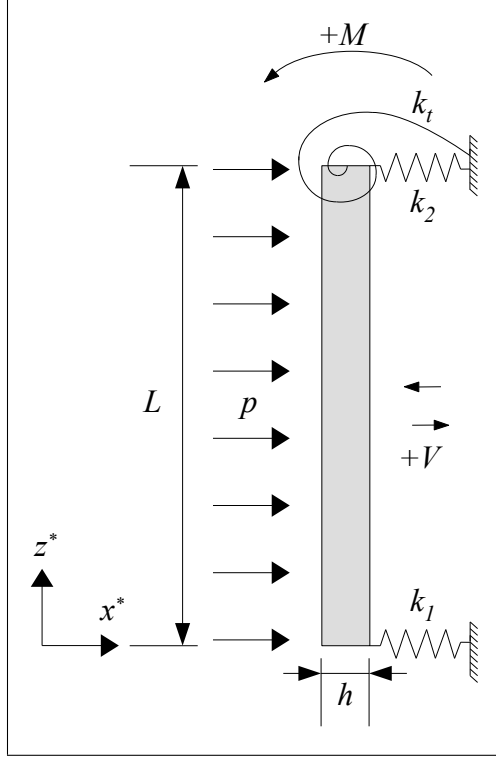


Figure 2.1: Draft portion of the water-impacted panel.

the top edge of the plate to compensate for any displacement that the stiffness of the upper, non-draft portion of the plate may prevent. A translational spring produces a restoring force of the form  $F = -kw^*$  along the panel of the plate to which it is parallel, the effective shear force at the plate boundary equals the translational spring's restoring force [19]. Using the shear force sign convention indicated in Fig. 2.1, the shear force boundary conditions are

$$D \frac{\partial^3 w^*}{\partial z^{*3}} \Big|_{z^*=0} + k_1^* w^* \Big|_{z^*=0} = 0, \quad (2.7)$$

$$-D \frac{\partial^3 w^*}{\partial z^{*3}} \Big|_{z^*=L} + k_2^* w^* \Big|_{z^*=L} = 0. \quad (2.8)$$

The shear force sign convention in Fig. 2.1 is reversed compared to the typical clockwise convention due to the axis of displacement ( $x^*$  in this case) pointing opposite to that in the typical convention.

A fictitious torsional spring  $k_t$  is also added at the top edge of the plate to compensate for any rotation that the stiffness of the upper, non-draft portion of the plate may prevent. The effect of the torsional spring at the top of the plate are specified as a natural boundary condition of the effective

bending moment. The torsional spring produces a restoring moment of the form  $\tau = -k\theta^*$  about the  $y$  direction at its edge of the plate. At this edge, the bending moment equals the restoring moment of the torsional spring. Using the bending moment sign convention in Fig. 2.1 and the small-angle approximation  $\theta^* \approx \partial w^*/\partial z^*$ , the bending moment boundary conditions are [15]

$$D \frac{\partial^2 w^*}{\partial z^{*2}} \Big|_{z^*=0} = 0, \quad (2.9)$$

$$D \frac{\partial^2 w^*}{\partial z^{*2}} \Big|_{z^*=L} + k_t^* \frac{\partial w^*}{\partial z^*} \Big|_{z^*=L} = 0. \quad (2.10)$$

The stiffnesses of these springs are determined using finite element models (see chapter 3)

The initial conditions are an initial position of  $x^* = 0$  and initial velocity in the  $+x^*$  direction of  $\dot{w}^* = u_0^*$  for the entire plate:

$$w^*|_{t^*=0} = 0, \quad (2.11)$$

$$\frac{\partial w^*}{\partial t^*} \Big|_{t^*=0} = u_0^*. \quad (2.12)$$

### 2.1.3. Nondimensionalized Model

The model is nondimensionalized to reduce the number of parameters and aid in the representation of the results. The nondimensional variables, which have no superscript asterisk, are defined as

$$t = \frac{t^*}{t_p}, \quad z = \frac{z^*}{L}, \quad w = \frac{w^*}{h}, \quad k_{1,2} = \frac{L^3}{D} k_{1,2}^*, \quad k_t = \frac{L^2}{D} k_t^*, \quad u_0 = \frac{t_p}{h} u_0^*,$$

where  $t_p$  is a characteristic time period of the plate [15],

$$t_p = L^2 \sqrt{\frac{\rho_p h}{D}}.$$

Thus, we can introduce the characteristic speed of sound,

$$c_p = \frac{L}{t_p}.$$

Substitution into Eq. 2.6 yields the nondimensionalized governing equation,

$$\frac{\partial^2 w(z, t)}{\partial t^2} + a \frac{\partial w(z, t)}{\partial t} + \frac{\partial^4 w(z, t)}{\partial z^4} = f, \quad (2.13)$$

where there are now two nondimensional parameters,

$$a = \frac{\rho_w c_w L}{\rho_p c_p h}, \quad f = \frac{\rho_w c_w u_0^* L^2}{\rho_p c_p^2 h^2} = a u_0.$$

Eq. 2.13, like Eq. 2.6, has the form of a Kirchhoff-Love plate under viscous damping and a constant uniform load. The nondimensionalized boundary conditions are

$$\left. \frac{\partial^3 w}{\partial z^3} \right|_{z=0} + k_1 w|_{z=0} = 0, \quad (2.14)$$

$$-\left. \frac{\partial^3 w}{\partial z^3} \right|_{z=1} + k_2 w|_{z=1} = 0, \quad (2.15)$$

$$\left. \frac{\partial^2 w}{\partial z^2} \right|_{z=0} = 0, \quad (2.16)$$

$$\left. \frac{\partial^2 w}{\partial z^2} \right|_{z=1} + k_t \left. \frac{\partial w}{\partial z} \right|_{z=1} = 0. \quad (2.17)$$

The nondimensionalized initial conditions are

$$w|_{t=0} = 0, \quad (2.18)$$

$$\left. \frac{\partial w}{\partial t} \right|_{t=0} = u_0. \quad (2.19)$$

## 2.2. Analytical Solution

The solution of Eqs. 2.13-2.19 is found by separation of variables [14, 19]. Let

$$w(z, t) = W(z) q(t), \quad (2.20)$$

where  $W(x)$  is the mode shape function, and  $q(t)$  represents the modal coordinates. It is assumed that the load  $f$  takes the form of the mode shape function multiplied by some function of time, i.e.,

$$f(z, t) = W(z) f_t(t). \quad (2.21)$$

Substituting Eqs. 2.20 and 2.21 into Eq. 2.13, dividing by  $Wq$ , and rearranging gives

$$\frac{1}{W} \frac{\partial^4 W}{\partial z^4} = -\frac{1}{q} \frac{\partial^2 q}{\partial t^2} - \frac{a}{q} \frac{\partial q}{\partial t} + \frac{f_t}{q}. \quad (2.22)$$

This states that two functions involving separate independent variables are equal to each other. Since each function does not vary with the other's independent variable, both functions must be equal to some constant. Therefore,

$$\frac{1}{W} \frac{\partial^4 W}{\partial z^4} = -\frac{1}{q} \frac{\partial^2 q}{\partial t^2} - \frac{a}{q} \frac{\partial q}{\partial t} + \frac{f_t}{q} = \omega^2, \quad (2.23)$$

where  $\omega$  is a constant. Thus,  $W(x)$  and  $q(t)$  are found from two separate ordinary differential equations,

$$\frac{d^4 W}{dz^4} - \beta^4 W = 0, \quad (2.24)$$

where  $\beta^4 = \omega^2$ , and

$$\frac{d^2 q}{dt^2} + a \frac{dq}{dt} + \omega^2 q = f_t. \quad (2.25)$$

The solution of Eq. 2.24 is found by assuming that

$$W(z) = C e^{sz}, \quad (2.26)$$

where  $C$  and  $s$  are constants. Substituting Eq. 2.26 into Eq. 2.24 yields the characteristic equation

$$s^4 - \beta^4 = 0,$$

whose four roots are

$$s = \pm\beta, \pm i\beta.$$

Substituting Eq. 2.26 with these roots into Eq. 2.24 yields, by superposition, the general solution,

$$W(z) = C_1 e^{\beta z} + C_2 e^{-\beta z} + C_3 e^{i\beta z} + C_4 e^{-i\beta z}, \quad (2.27)$$

or

$$W(z) = C_1 \sin(\beta z) + C_2 \cos(\beta z) + C_3 \sinh(\beta z) + C_4 \cosh(\beta z), \quad (2.28)$$

where  $C_1$ ,  $C_2$ ,  $C_3$ , and  $C_4$  are known as mode shape coefficients. Substituting Eq. 2.28 into the four boundary conditions 2.14-2.17 yields an eigenvalue problem of the form

$$\mathbf{A} \begin{bmatrix} C_1 \\ C_2 \\ C_3 \\ C_4 \end{bmatrix} = \begin{bmatrix} 0 \\ 0 \\ 0 \\ 0 \end{bmatrix}, \quad (2.29)$$

where

$$\mathbf{A} = \begin{bmatrix} -\beta^3 & k_1 & \beta^3 & k_1 \\ 0 & -\beta & 0 & \beta^2 \\ -\beta^3 \cos(\beta) - k_2 \sin(\beta) & \beta^3 \sin(\beta) - k_2 \cos(\beta) & \beta^3 \cosh(\beta) - k_2 \sinh(\beta) & \beta^3 \sinh(\beta) - k_2 \cosh(\beta) \\ \beta k_t \cos(\beta) - \beta^2 \sinh(\beta) & -\beta^2 \cos(\beta) - \beta k_t \sin(\beta) & \beta k_t \cosh(\beta) + \beta^2 \sinh(\beta) & \beta^2 \cosh(\beta) + \beta k_t \sinh(\beta) \end{bmatrix}. \quad (2.30)$$

The determinant of  $\mathbf{A}$  set equal to zero is called the frequency equation, which is a function of  $\beta$ . The roots of the frequency equation,  $\beta_n$ , where  $n = 1, 2, 3, \dots$ , which are the eigenvalues, are found numerically. Therefore, the  $n$ th mode shape is

$$W_n(z) = C_{1,n} \sin(\beta_n z) + C_{2,n} \cos(\beta_n z) + C_{3,n} \sinh(\beta_n z) + C_{4,n} \cosh(\beta_n z). \quad (2.31)$$

From Eq. 2.25, it can be seen that  $\beta_n$  is the square-root of the natural angular frequency,  $\omega$ , of the  $n$ th mode shape.

Since the matrix  $\mathbf{A}$  is made singular by the roots  $\beta_n$ , unique values of the eigenvectors involving  $C_{1,n}$ ,  $C_{2,n}$ ,  $C_{3,n}$ , and  $C_{4,n}$  cannot be found. Instead, three of these four coefficients are considered to be amplitude ratios with respect to the remaining one, chosen arbitrarily [14]. For example, Eq. 2.31 can be rewritten as

$$W_n(z) = C_{1,n} \left[ \sin(\beta_n z) + \frac{C_{2,n}}{C_{1,n}} \cos(\beta_n z) + \frac{C_{3,n}}{C_{1,n}} \sinh(\beta_n z) + \frac{C_{4,n}}{C_{1,n}} \cosh(\beta_n z) \right].$$

Setting one of the coefficients equal to 1, the remaining three coefficients can be computed. If any such  $3 \times 3$  submatrix is found to be singular, a different coefficient can be set equal to 1. If a value other than 1 were chosen for the arbitrary coefficient, this constant would have to be taken into account when applying the initial conditions to find  $q(t)$ . The method of computing the mode shape coefficients can be verified by comparing to known values for classical boundary conditions [31], such as fixed, free, or pinned edges, by using appropriate combinations of zero or very large values for the spring stiffnesses.

It can now be seen that the solution of 2.20 must be a summation involving multiple mode shapes,  $W_n(z)$ . Thus, Eq. 2.20 is expressed as a linear combination of the mode shapes, that is,

$$w(z, t) = \sum_{n=1}^{\infty} W_n(z) q_n(t). \quad (2.32)$$

This is a series expansion known as an orthogonal series [25]. It can be shown that the mode shape functions are orthogonal functions [14], that is,

$$\int_0^1 W_n(z) W_m(z) dz = 0, \quad n \neq m. \quad (2.33)$$

Thus, the only nonzero such integrals are

$$\int_0^1 W_n^2(z) dz \neq 0, \quad n = 1, 2, \dots \quad (2.34)$$

From Eq. 2.32, the plate's initial velocity, given by Eq. 2.19, is

$$\dot{w}(z, 0) = u_0 = \sum_{n=1}^{\infty} W_n(z) \dot{q}_n(0). \quad (2.35)$$

If both sides of Eq. 2.35 are multiplied by  $W_n(z)$  and integrated over the length of the plate, then making use of the orthonality conditions expressed in Eqs. 2.33 and 2.34,

$$\dot{q}_n(0) = \frac{u_0 \int_0^1 W_n(z) dz}{\int_0^1 W_n^2(z) dz}, \quad (2.36)$$

where  $u_0$  is moved outside the integral since it is independent of  $z$  in this problem.

Similarly, it is assumed that Eq. 2.21 can be expressed as the linear combination

$$f = \sum_{n=1}^{\infty} W_n(z) f_{t,n}(t), \quad (2.37)$$

where  $f(z, t)$  is now simply  $f$  since it is independent of  $z$  and  $t$  in this problem. Therefore,

$$f_{t,n} = \frac{f \int_0^1 W_n(z) dz}{\int_0^1 W_n^2(z) dz}, \quad (2.38)$$

where  $f_{t,n}(t)$  is now simply  $f_{t,n}$  since it is independent of time in this problem.

The solution of Eqs. 2.25, 2.18 and 2.19 for each mode is

$$q_n(t) = \frac{[(2\omega_n^2 \dot{q}_n(0) - a f_{t,n}) \sin(\frac{d}{2}t) - f_{t,n}d (\cos(\frac{d}{2}t) - e^{at/2})] e^{-at/2}}{d}, \quad (2.39)$$

where  $d = \sqrt{a^2 - 4\omega_n^2}$ .

Finally, the solution of Eqs. 2.13-2.19 is computed using Eq. 2.32 with a finite number of modes:

$$w(z, t) = \sum_{n=1}^N W_n(z) q_n(t), \quad (2.40)$$

from Eqs. 2.31 and 2.39. The solution becomes increasingly accurate as more modes are computed.

# Chapter 3

## Numerical Validation

### 3.1. The Draft-Portion Model (DPM)

The analytical model was validated using finite element models. Two different finite element models were developed. The first, called the *draft-portion model*, or DPM, models the same plate as the analytical model.<sup>1</sup> The purpose of this model is to validate the analytical model matching displacement, velocity, and acceleration data with those of the analytical model. Modeling only the draft-portion of the plate, the DPM contains the translational spring  $k_1$  and the fictitious translational spring  $k_2$  and fictitious torsional spring  $k_t$ .

### 3.2. The Full-Plate Model (FPM)

The second finite element model developed is the *full-plate model* (Fig. 3.1), or FPM, which models the entire water-impacted panel of the shipping container. The FPM was used to ensure that values of  $k_2$  and  $k_t$  in the DPM can be chosen such that points along the DPM's plate match the displacement of the equivalent points along the draft portion of the full plate. Thus, the FPM was used to validate that the analytical model is applicable to this particular problem. It was also used to visualize the displacement of the entire water-impacted panel. The FPM is simply an extension of the DPM, in that the FPM was created from the DPM, but with a plate length of  $L_f$  equal to the height of a shipping container, and with the damping and constant acoustic load  $p$  applied over only the length  $L$ .

As indicated in Fig. 3.1, the FPM contains only the two translational springs at the top and bottom of the plate with stiffnesses  $k_1$  and  $k_3$ . That is, it models the whole water-impacted panel of the shipping container, where the two springs represent the upper and lower panels of the shipping container. Specifically, these springs represent the stiffness of the upper and lower rails in the shipping container, which contribute most of the stiffness (see chapter 4).

1. Although the analytical model also represents only the draft-portion of the plate, "DPM" is used to refer to this finite element model only.

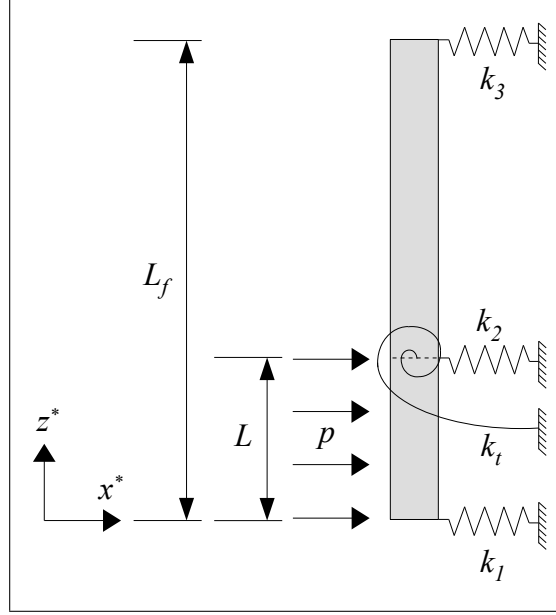


Figure 3.1: The draft-portion model within the full-plate model.

The dimensional stiffnesses  $k_2^*$  and  $k_t^*$  in the DPM were chosen by trial and error such that the DPM and FPM yielded similar displacements at the points  $z = 0$ ,  $z = 1/2$  and  $z = 1$  ( $z = 1$  corresponds to  $z^* = L$ ) along the plate. These stiffnesses were then used in the analytical model, which models the draft portion only.

### 3.3. Description of the Finite Element Models

The purpose of this subsection is to describe the salient aspects of the model in enough detail such that the models could be reproduced by the reader. An exhaustive derivation of the procedures is not provided since the finite element models are not the main goal of this research. The finite element models were written in GNU Octave [5], mostly based on code adapted from Ferreira and Fantuzzi [6].

The displacement of the plate is interpolated using the Hermite interpolation functions [13],

$$N_1(z_e^*) = 1 - 3\left(\frac{z_e^*}{L_e}\right)^2 + 2\left(\frac{z_e^*}{L_e}\right)^3, \quad (3.1)$$

$$N_2(z_e^*) = z_e^* - \frac{2z_e^{*2}}{L_e} + \frac{3z_e^{*3}}{L_e^2}, \quad (3.2)$$

$$N_3(z_e^*) = 3 \left( \frac{z_e^*}{L_e} \right)^2 - 2 \left( \frac{z_e^*}{L_e} \right)^3, \quad (3.3)$$

$$N_4(z_e^*) = -\frac{z_e^{*2}}{L_e} + \frac{z_e^{*3}}{L_e^2}, \quad (3.4)$$

where  $z_e^*$  is the local  $z^*$  coordinate along an element of length  $L_e$ . In the matrix form

$$\mathbf{N} = \begin{bmatrix} N_1 & N_2 & N_3 & N_4 \end{bmatrix}. \quad (3.5)$$

The element displacement vector is

$$\mathbf{w}^e = \begin{bmatrix} w_1 \\ \frac{\partial w_1}{\partial z_e^*} \\ w_2 \\ \frac{\partial w_2}{\partial z_e^*} \end{bmatrix}, \quad (3.6)$$

where  $w_1$  and  $w_2$  are the transverse displacements of the element's two nodes, and the partial derivatives are the slopes. Both the mass and damping matrices contain the common element matrix

$$\mathbf{N}^e = \int_0^{L_e} \mathbf{N}^T \mathbf{N} dz_e^* = \frac{L_e}{420} \begin{bmatrix} 156 & 22L_e & 54 & -13L_e \\ 22L_e & 4L_e^2 & 13L_e & -3L_e^2 \\ 54 & 13L_e & 156 & -22L_e \\ -13 & -3L_e^2 & -22L_e & 4L_e^2 \end{bmatrix}. \quad (3.7)$$

The element consistent mass matrix is

$$\mathbf{M}^e = \rho_p h \mathbf{N}^e. \quad (3.8)$$

Similarly, the element consistent damping matrix is [32]

$$\mathbf{C}^e = \rho_w c_w \mathbf{N}^e. \quad (3.9)$$

The element stiffness matrix is

$$\mathbf{K}^e = D \int_0^{L_e} \mathbf{N}''^T \mathbf{N}'' dz_e^* = \frac{D}{L_e^3} \begin{bmatrix} 12 & 6L_e & -12 & 6L_e \\ 6L_e & 4L_e^2 & -6L_e & 2L_e^2 \\ -12 & -6L_e & 12 & -6L_e \\ 6L_e & 2L_e^2 & -6L_e & 4L_e^2 \end{bmatrix}. \quad (3.10)$$

The element force vector is

$$\mathbf{f}^e = \rho_p c_w u_0^* \int_0^{L_e} \mathbf{N} dz_e^* = \rho_p c_w u_0^* \begin{bmatrix} L_e/2 \\ L_e^2/12 \\ L_e/2 \\ -L_e^2/12 \end{bmatrix}. \quad (3.11)$$

The global mass matrix  $\mathbf{M}$ , global damping matrix  $\mathbf{C}$ , global stiffness matrix  $\mathbf{K}$ , and global force vector  $\mathbf{f}$  are then assembled. The spring stiffnesses are added to the global stiffness matrix at the appropriate nodes and at separate fixed nodes to which the springs are attached. Thus, the matrix equation

$$\mathbf{M}\ddot{\mathbf{w}} + \mathbf{C}\dot{\mathbf{w}} + \mathbf{K}\mathbf{w} = \mathbf{f} \quad (3.12)$$

can be solved using Newmark's method, which yields a time history of the displacement, velocity, and acceleration of each node in the matrices  $\mathbf{w}$ ,  $\dot{\mathbf{w}}$ , and  $\ddot{\mathbf{w}}$ , respectively. The Newmark method in [6] was modified to include the damping term in Eq. 3.12 as described in Reddy [20]. Newmark parameters of  $\alpha = 3/2$  and  $\gamma = 2\beta = 2$ , as presented in Reddy [20], were used since these produced better visual agreement with the analytical model than other alternatives.

# Chapter 4

## Results

### 4.1. Stiffnesses of the Bottom and Top of the Shipping Container

Before results can be computed from the models, values for the stiffnesses  $k_1$  and  $k_3$ , representing the bottom and top sides of the shipping container, must be obtained. It is assumed that the vast majority of the stiffness of these sides of the container is provided by the top panel, along with the various steel rails connected to the water-impacted panel. The dimensions of these rails are given in [2]. It is assumed that the wooden floor does not contribute significantly to the bottom stiffness. The left and right side panels are not considered.

Pertaining to the bottom stiffness,  $k_1$ , the cross-sectional area of each of the two bottom side rails, and that of the longitudinal floor beam are

$$A_{\text{bot. rail}} = (0.005 \text{ m}) (0.0513 \text{ m} + 0.0304 \text{ m} + 0.0254 \text{ m} + 0.127 \text{ m} + 0.0317 \text{ m}), \quad (4.1)$$

and

$$A_{\text{floor beam}} = (0.0028 \text{ m}) (4 \times 0.0254 \text{ m} + 0.0445 \text{ m}). \quad (4.2)$$

Therefore,

$$k_1 = \frac{E (2A_{\text{bot. rail}} + A_{\text{floor beam}})}{L_c}, \quad (4.3)$$

where  $L_c$  is the length of the container (6.05 m for the 20-foot, or 12.19 m for the 40-foot container [28]). For the 20-foot container,  $k_1 \approx 1.01 \times 10^8$  N/m, and for the 40-foot container,  $k_1 \approx 5.03 \times 10^7$  N/m.

Pertaining to the top stiffness,  $k_3$ , the cross-sectional area of each of the two top side rails is

$$A_{\text{top rail}} = (0.003 \text{ m}) (2 \times 0.0603 \text{ m} + 2 \times 0.0445 \text{ m}). \quad (4.4)$$

Because the panels of the container are made of 2 mm 14-gauge steel, the cross-sectional area of the top panel is

$$A_{\text{top panel}} = 0.002 \text{ m} \times 1 \text{ m}, \quad (4.5)$$

since plate theory expresses the horizontal direction along the plate as a unit length. Therefore,

$$k_3 = \frac{E(2A_{\text{top rail}} + A_{\text{top panel}})}{L_c}. \quad (4.6)$$

For the 20-foot container,  $k_3 \approx 1.08 \times 10^8$  N/m, and for the 40-foot container,  $k_3 \approx 5.34 \times 10^7$  N/m.

## 4.2. Results from the Models

Results were computed for the six cases of the 20-foot shipping container and 40-foot shipping container at 100%, 50%, and 0% of their maximum cargo capacities based on specifications given in [28]. The values common to all six cases are:

$\rho_p = 7850$  kg/m<sup>3</sup>, the density of steel [12];

$h = 2$  mm, the thickness of the container's 14-gauge steel walls [4, 22];

$\rho_w = 1025$  kg/m<sup>3</sup>, the density of seawater [12];

$c_w = 1560$  m/s, the speed of sound in seawater [12];

$u_0^* = 6$  m/s, the speed of the tsunami inundation water flow [12];

$E = 200$  GPa, Young's modulus of steel [2];

$\nu = 0.3$ , Poisson's ratio for steel [2];

$L_f = 2.59$  m, the length of the water-impacted panel of the shipping container [28].

For each case, the length of the draft portion of the plate,  $L$ , was calculated from Archimedes' principle. The equations simplify to

$$L = \frac{\rho_{con}}{\rho_w} L_f, \quad (4.7)$$

where

$$\rho_{con} = \frac{m_{con}}{V_{con}}, \quad (4.8)$$

in which  $\rho_{con}$ ,  $m_{con}$  and  $V_{con}$  are the density, mass and volume, respectively, of the shipping container. The volume of the 20-foot container is  $V_{con} = 6.05 \text{ m} \times 2.44 \text{ m} \times 2.59 \text{ m} \approx 38.23 \text{ m}^3$ , and the volume of the 40-foot container is  $V_{con} = 12.19 \text{ m} \times 2.44 \text{ m} \times 2.59 \text{ m} \approx 77.03 \text{ m}^3$  [28].

The analytical solution was computed using the software SageMath [23]. Arbitrary precision is necessary for computing most of the roots of the frequency equation using bisection. The DPM used 4,000 time steps to achieve visual agreement with the analytical model.

For each of the six cases, the following results are given:

- 1) The comparison of the finite element DPM and FPM, which allows appropriate values of  $k_2$  and  $k_t$  to be chosen (see section 3.2).
- 2) Numerical values of  $\beta_n$ ,  $C_{1,n}$ ,  $C_{3,n}$ ,  $\dot{q}_n(0)$ , and  $f_{t,n}$  yielded by the analytical model for the first five modes.  $C_{2,n}$  and  $C_{4,n}$  are always 1.
- 3) Comparisons of displacement, velocity, and acceleration between the analytical model and DPM, which validates the analytical model. These are given at three points along the length plate,  $z = 0$ ,  $z = 1/2$ , and  $z = 1$ .
- 4) A plot of the displacement at  $z = 0$  with a logarithmic time axis.
- 5) A two-dimensional representation of the displacement of the draft-portion plate over time given by the analytical model.
- 6) A two-dimensional representation of the displacement of the full plate over time given by the FPM using 200 elements.
- 7) The nondimensional relative acoustic load,  $a(u_0 - \dot{w})$ , over time. The graph at  $t = 1/200$  represents the first time step after  $t = 0$ .

Regarding point 1 above, the fictitious stiffnesses were found to be  $k_2^* = 0$  and  $k_t^* = 10^4$  N·m/rad for all cases, suggesting that the container's panel has a low rigidity, as modeled.

Following from section 2.1.3, the conversion factors for nondimensional-to-dimensional displacement, velocity, and acceleration, are  $h$ ,  $h/t_p$ , and  $h/t_p^2$ , respectively. The time duration was chosen to be twice the ratio of the length of the full plate to the speed of sound in the water,  $2L_f/c_w \approx 0.003$  s, since this is the same for both containers. The use of the speed of sound in water allows for comparisons to future work on the model that may include the acoustics in the water.

### 4.3. 20-Foot Container at 100% Capacity

The 20-foot shipping container at maximum capacity is now considered. Its mass is  $m_{con} = 24,000$  kg, which yields a draft length of  $L = 1.585$  m (about 61% of the full plate). This case used  $N = 120$  modes.

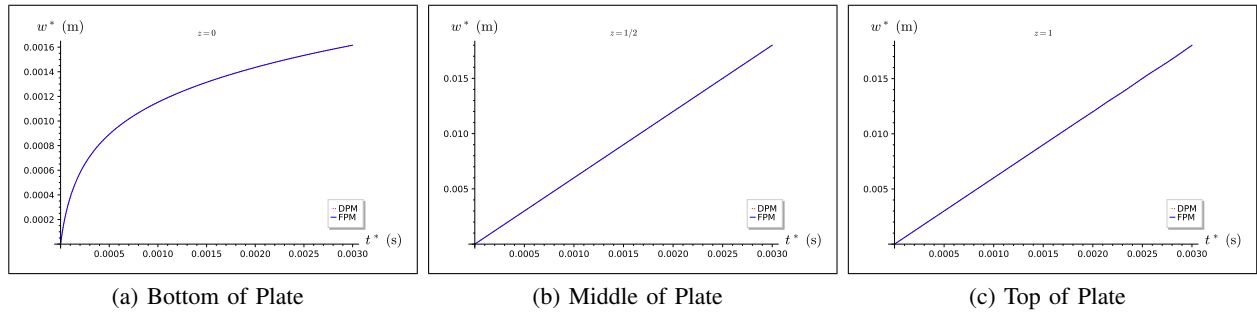


Figure 4.3.1: 20', 100%: displacement comparisons of finite element DPM and FPM.

Table 4.1: 20', 100%: analytical results.

$n$	$\beta_n$	$C_{1,n}$	$C_{3,n}$	$\dot{q}_n(0)$	$f_{t,n}$
1	1.5663	$1.44 \times 10^6$	2616.5	0.0021806	182.9
2	4.6989	53219	-14.08	0.019709	1653.1
3	7.8316	11497	-0.79652	0.054729	4590.4
4	10.964	4188.9	-1.0045	0.10731	9000.7
5	14.097	1970.3	-0.99988	0.17749	14887

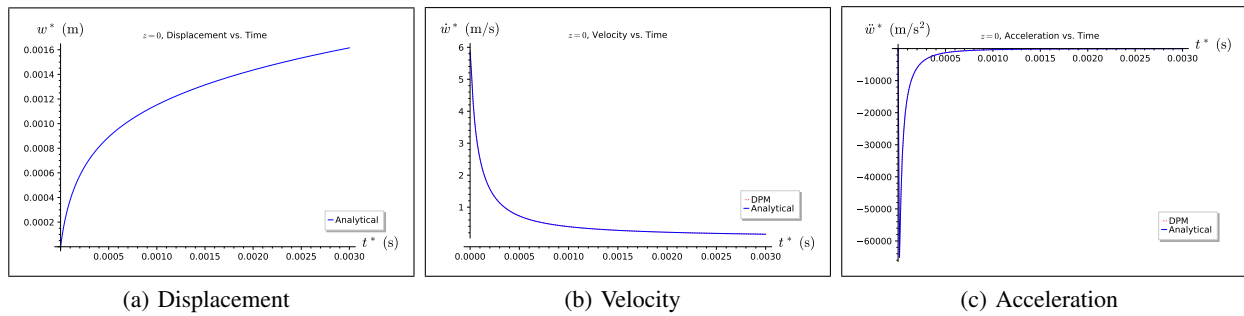


Figure 4.3.2: 20', 100%: comparison of analytical model and DPM at  $z = 0$ .

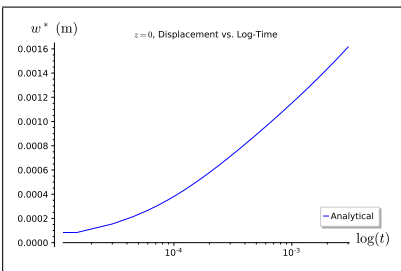
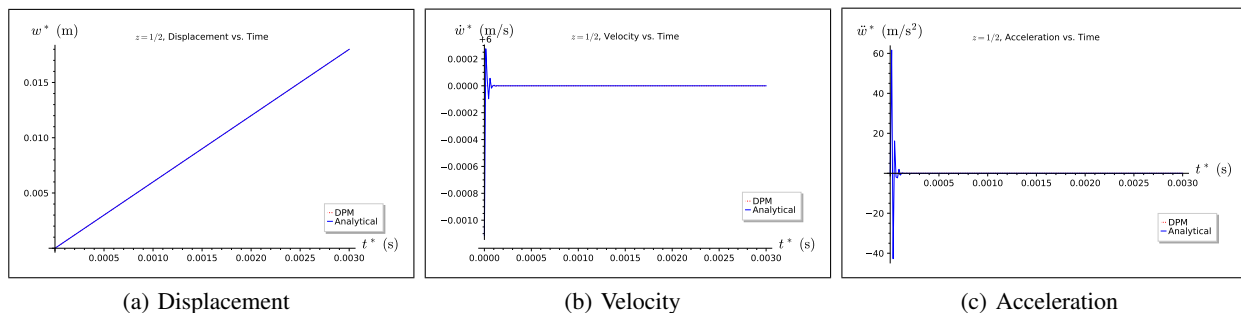
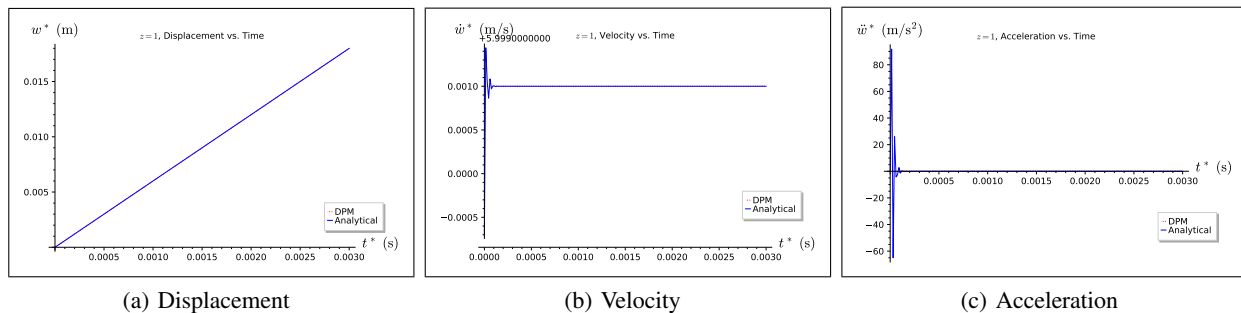


Figure 4.3.3: 20', 100%:  $z = 0$ , displacement vs. logarithm of time.



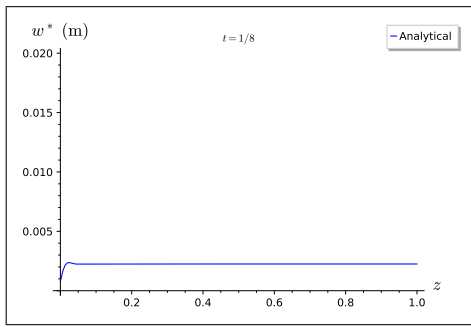
(a) Displacement (b) Velocity (c) Acceleration

Figure 4.3.4: 20', 100%: comparison of analytical model and DPM at  $z = 1/2$ .

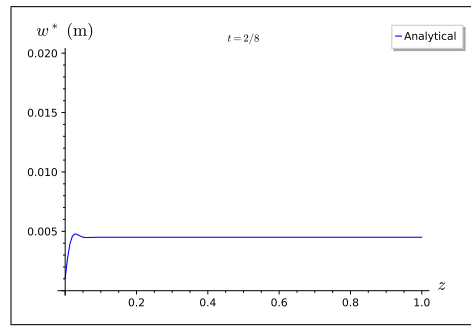


(a) Displacement (b) Velocity (c) Acceleration

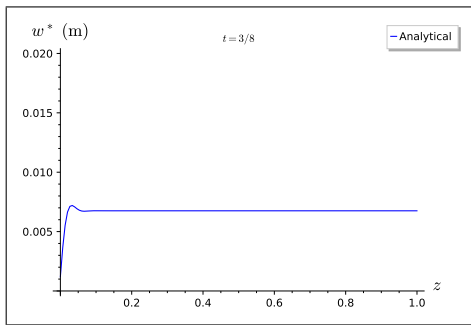
Figure 4.3.5: 20', 100%: comparison of analytical model and DPM at  $z = 1$ .



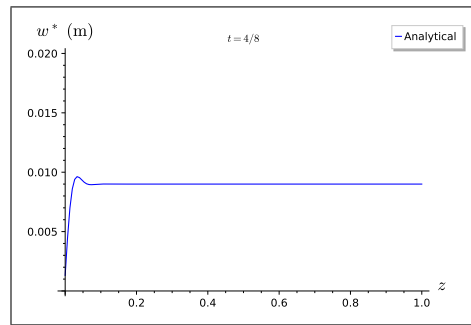
(a)  $t = 1/8$



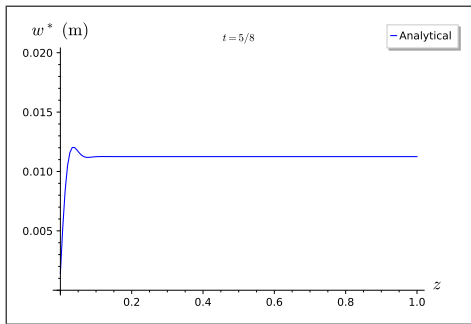
(b)  $t = 2/8$



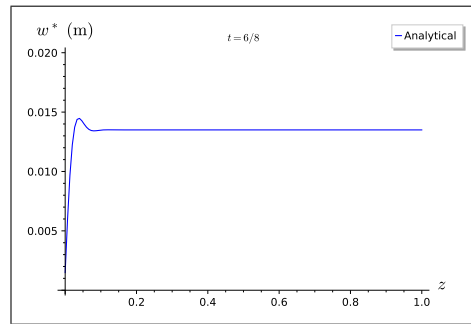
(c)  $t = 3/8$



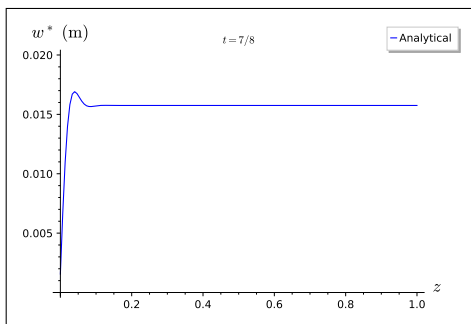
(d)  $t = 4/8$



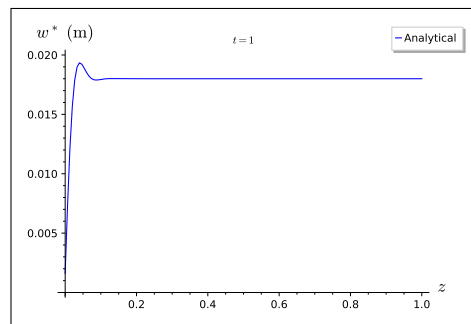
(e)  $t = 5/8$



(f)  $t = 6/8$

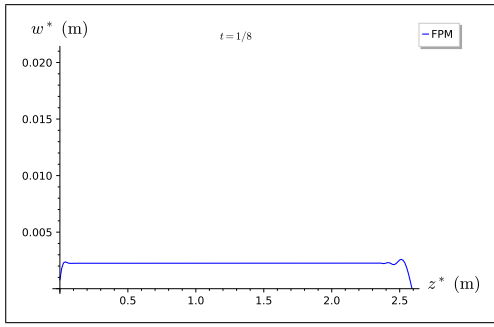


(g)  $t = 7/8$

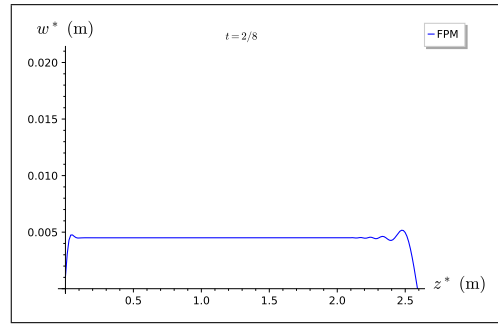


(h)  $t = 1$

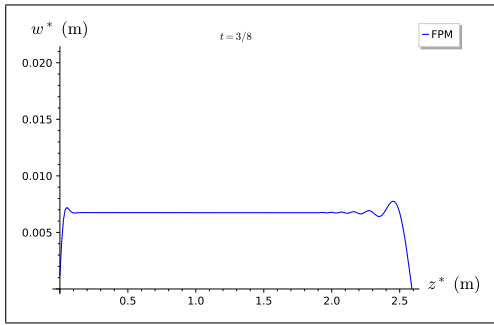
Figure 4.3.6: 20°, 100%: analytical 2-D displacement of the draft portion of the plate.



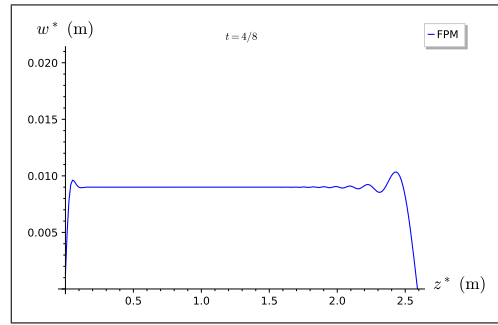
(a)  $t = 1/8$



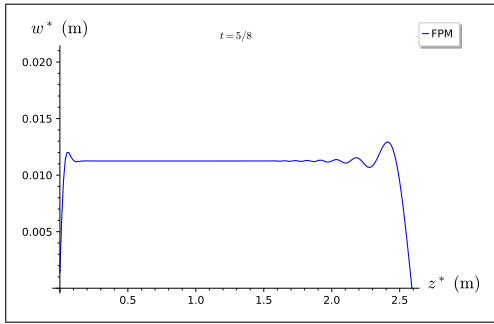
(b)  $t = 2/8$



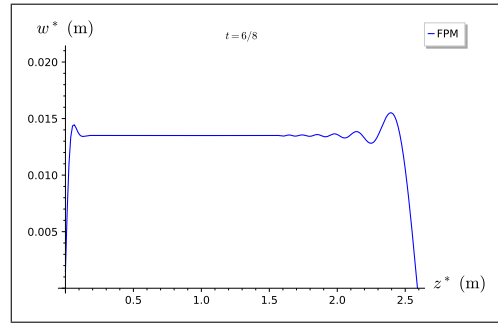
(c)  $t = 3/8$



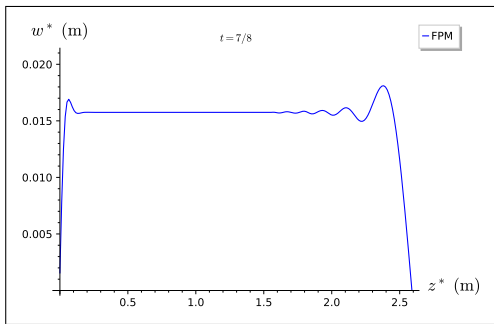
(d)  $t = 4/8$



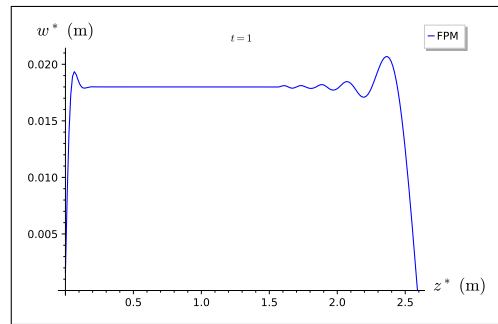
(e)  $t = 5/8$



(f)  $t = 6/8$

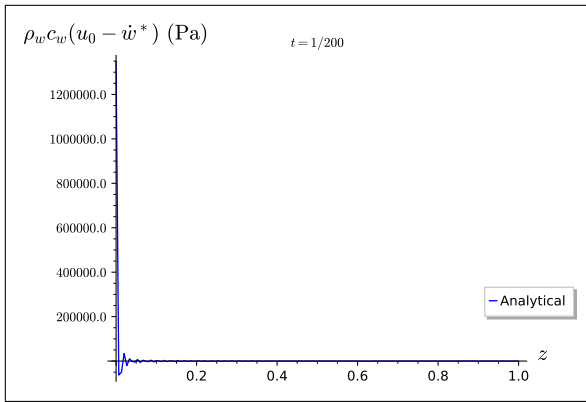


(g)  $t = 7/8$

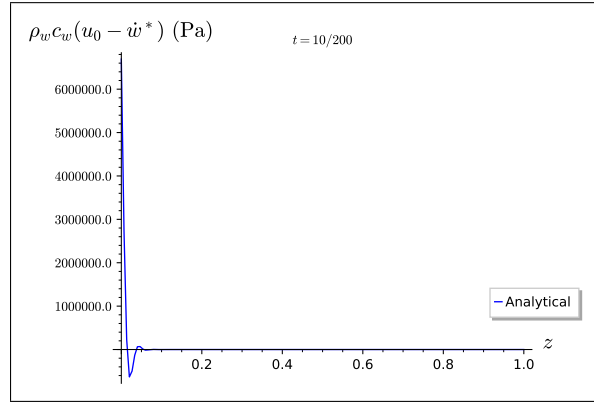


(h)  $t = 1$

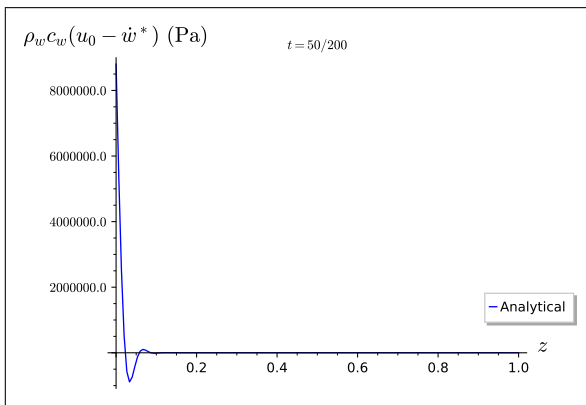
Figure 4.3.7: 20', 100%: FPM 2-D displacement of the full plate.



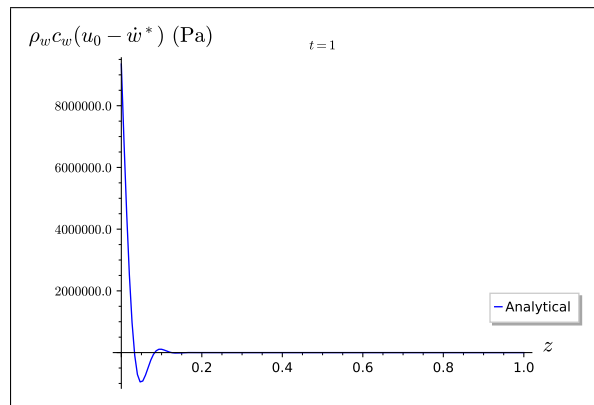
(a)  $t = 1/200$



(b)  $t = 10/200$



(c)  $t = 50/200$



(d)  $t = 1$

Figure 4.3.8: 20', 100%: relative acoustic load over the plate.

#### 4.4. 20-Foot Container at 50% Capacity

The 20-foot shipping container at half capacity is now considered. Its mass is  $m_{con} = 13,180$  kg, which yields a draft length of  $L = 0.871$  m (about 34% of the full plate). This case used  $N = 70$  modes.

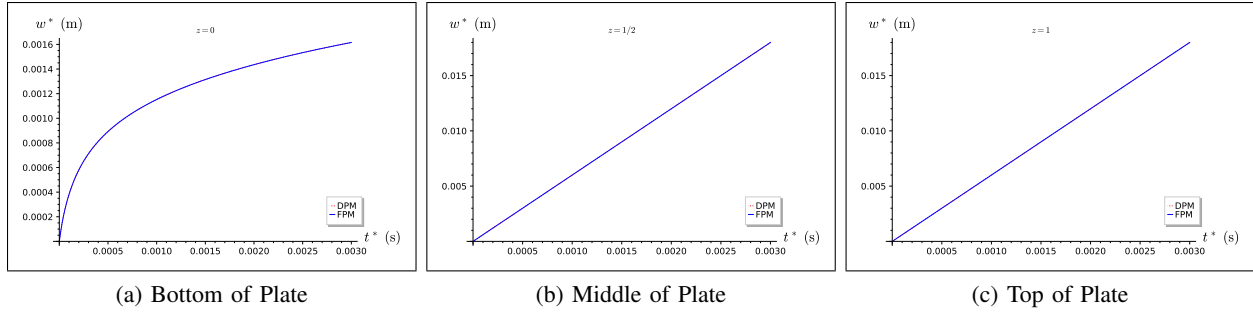


Figure 4.4.1: 20', 50%: displacement comparisons of finite element DPM and FPM.

Table 4.2: 20', 50%: analytical results.

$n$	$\beta_n$	$C_{1,n}$	$C_{3,n}$	$\dot{q}_n(0)$	$f_{t,n}$
1	1.5560	$2.4427 \times 10^5$	1461.4	0.0038612	97.67
2	4.6692	8977.5	-8.2578	0.03527	892.17
3	7.7837	1938.7	-0.88739	0.097963	2478
4	10.899	705.45	-1.0025	0.1925	4869.5
5	14.016	331.23	-0.99994	0.3194	8079.3

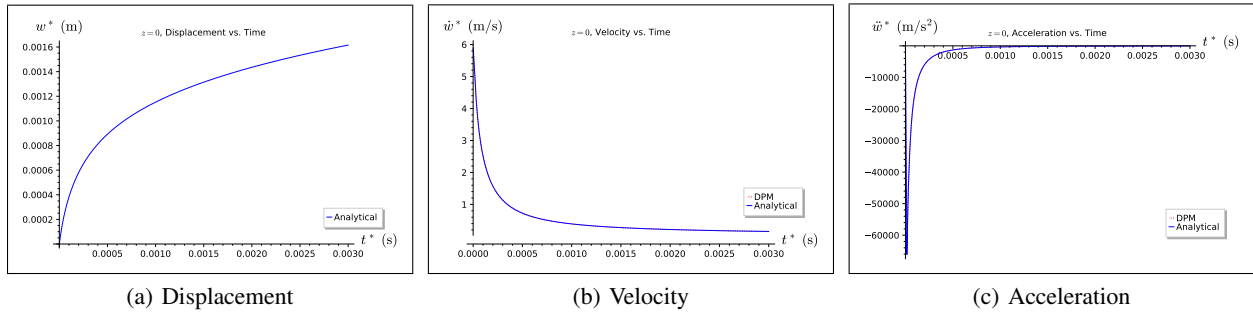


Figure 4.4.2: 20', 50%: comparison of analytical model and DPM at  $z = 0$ .

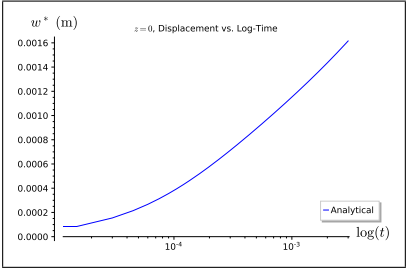


Figure 4.4.3: 20', 50%:  $z = 0$ , displacement vs. logarithm of time.

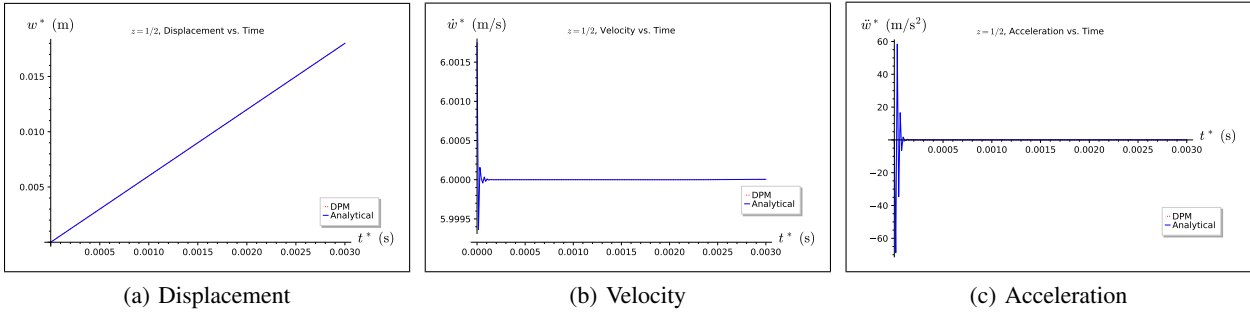


Figure 4.4.4: 20', 50%: comparison of analytical model and DPM at  $z = 1/2$ .

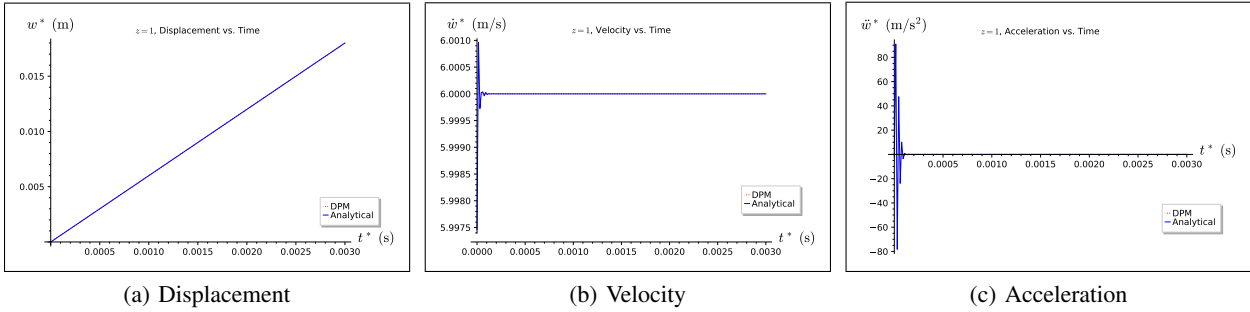
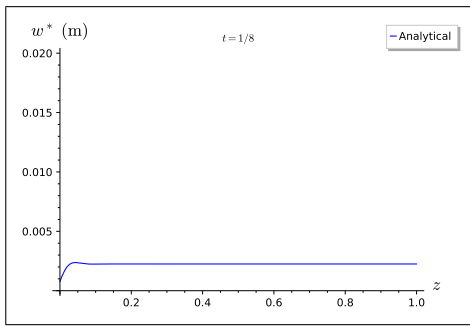
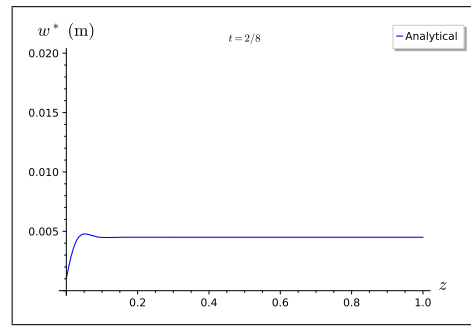


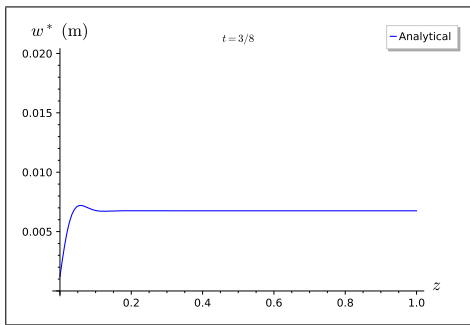
Figure 4.4.5: 20', 50%: comparison of analytical model and DPM at  $z = 1$ .



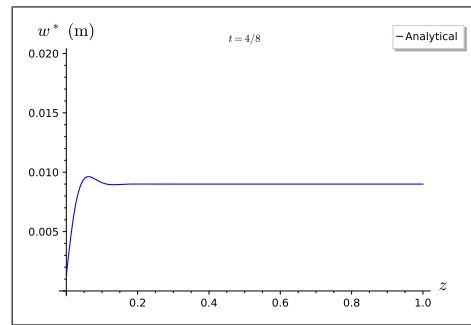
(a)  $t = 1/8$



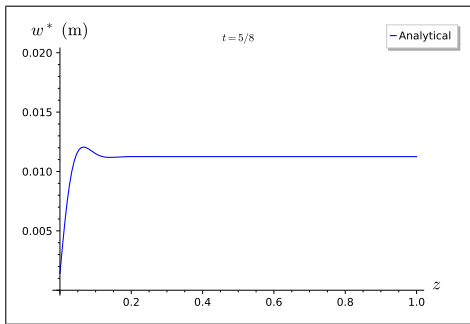
(b)  $t = 2/8$



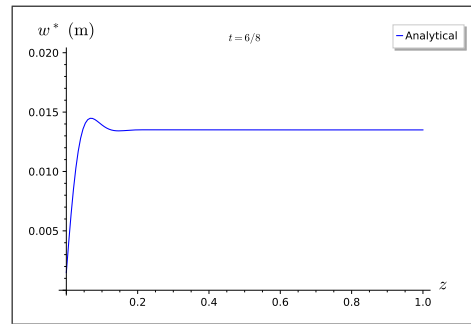
(c)  $t = 3/8$



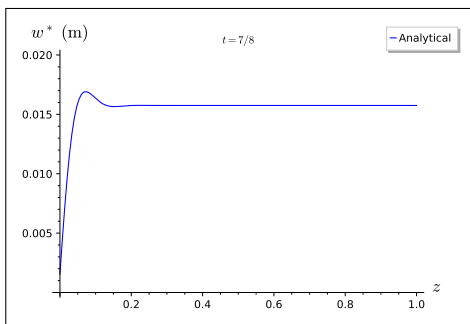
(d)  $t = 4/8$



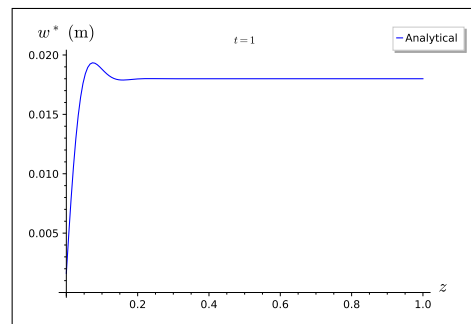
(e)  $t = 5/8$



(f)  $t = 6/8$

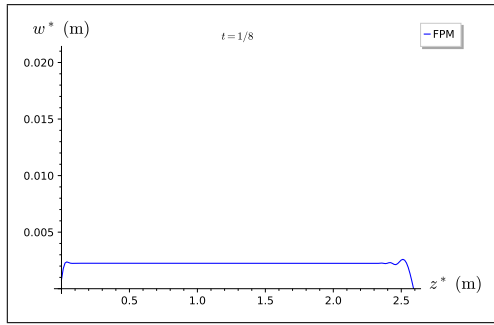


(g)  $t = 7/8$

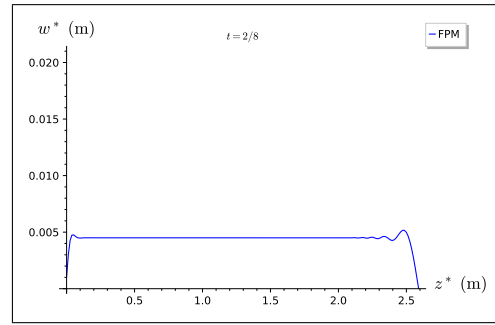


(h)  $t = 1$

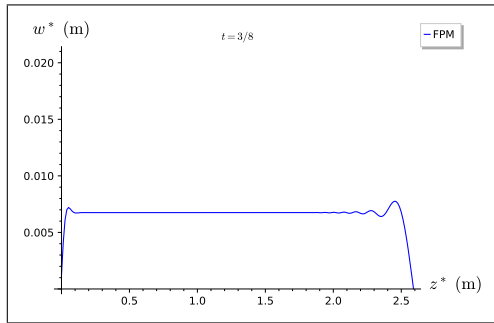
Figure 4.4.6: 20', 50%: analytical 2-D displacement of the draft portion of the plate.



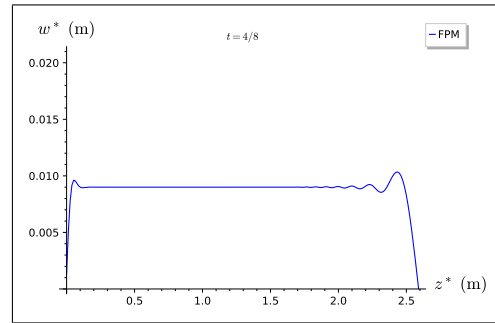
(a)  $t = 1/8$



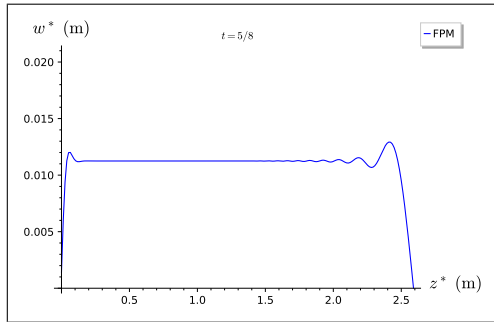
(b)  $t = 2/8$



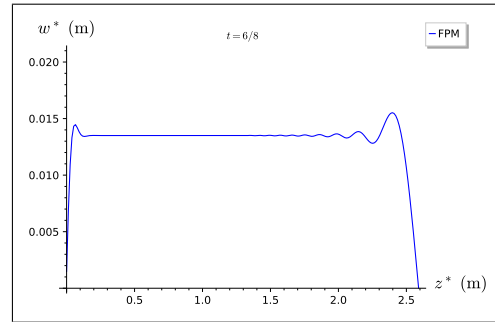
(c)  $t = 3/8$



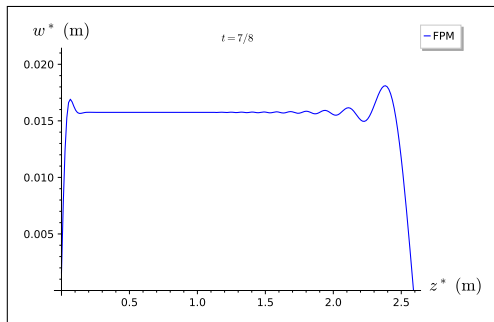
(d)  $t = 4/8$



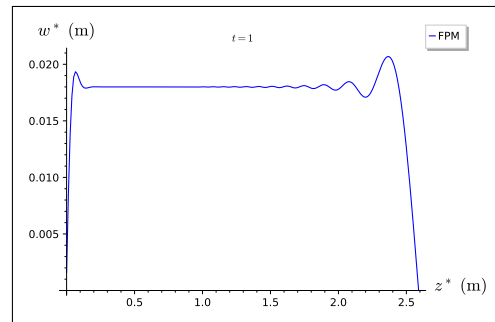
(e)  $t = 5/8$



(f)  $t = 6/8$

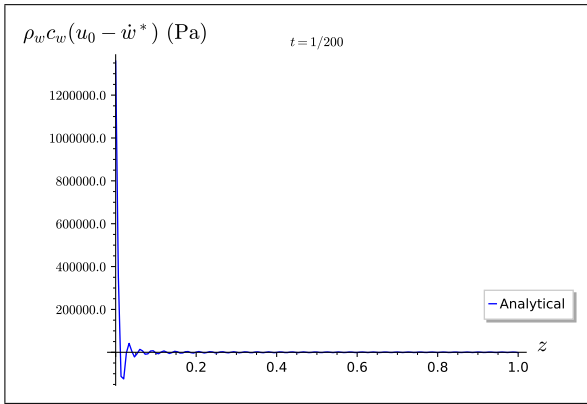


(g)  $t = 7/8$

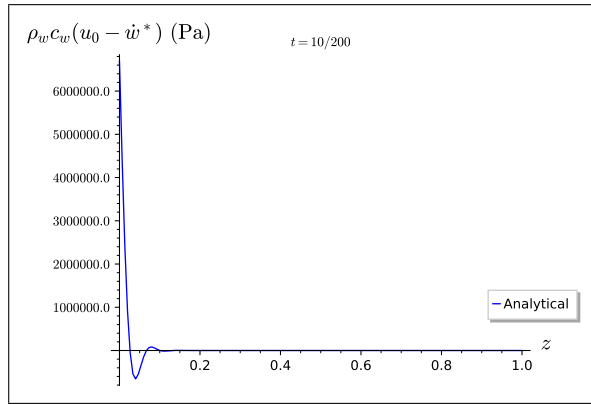


(h)  $t = 1$

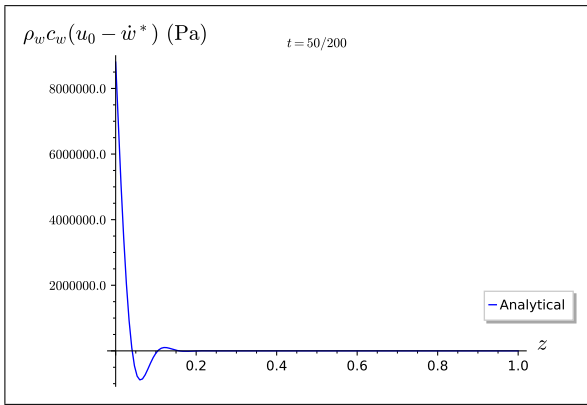
Figure 4.4.7: 20°, 50%: FPM 2-D displacement of the full plate.



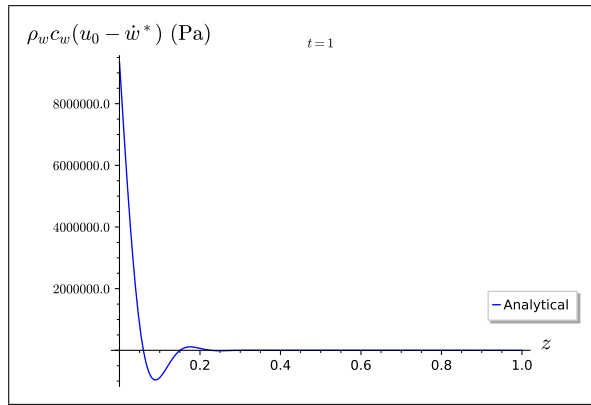
(a)  $t = 1/200$



(b)  $t = 10/200$



(c)  $t = 50/200$



(d)  $t = 1$

Figure 4.4.8: 20', 50%: relative acoustic load over the plate.

## 4.5. 20-Foot Container Empty

The empty 20-foot shipping container is now considered. Its mass is  $m_{con} = 2,360$  kg, which yields a draft of  $L = 0.156$  m (about 6% of the full plate). This case used  $N = 25$  modes.

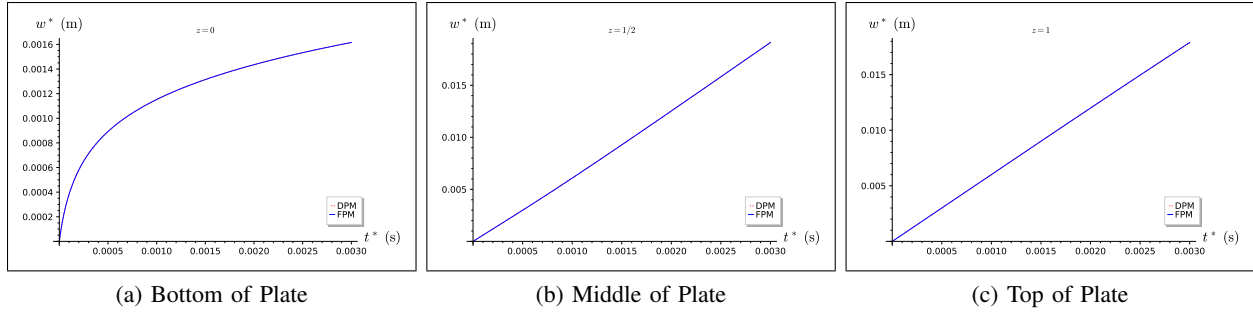


Figure 4.5.1: 20', empty: displacement comparisons of finite element DPM and FPM.

Table 4.3: 20', empty: analytical results.

$n$	$\beta_n$	$C_{1,n}$	$C_{3,n}$	$\dot{q}_n(0)$	$f_{t,n}$
1	1.2874	2871.4	410.42	0.009747	7.9051
2	4.1888	69.42	-2.0256	0.16026	129.98
3	7.1787	13.206	-0.9886	0.51081	414.28
4	10.110	4.0814	-1.0002	1.2396	1005.4
5	12.867	1.4652	-0.99999	2.4437	1981.9

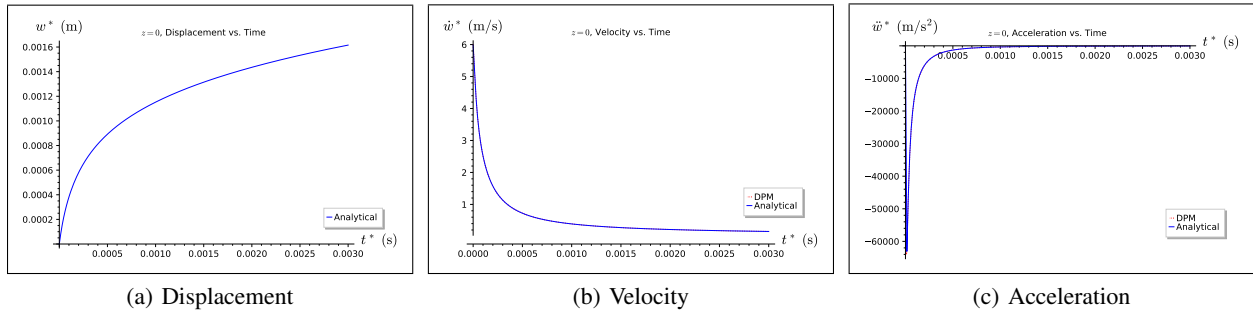


Figure 4.5.2: 20', empty: comparison of analytical model and DPM at  $z = 0$ .

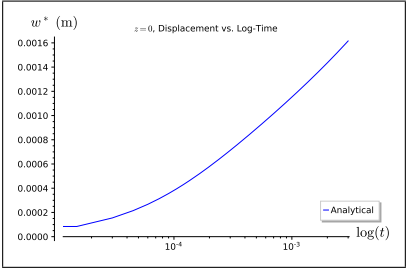


Figure 4.5.3:  $20'$ , empty:  $z = 0$ , displacement vs. logarithm of time.

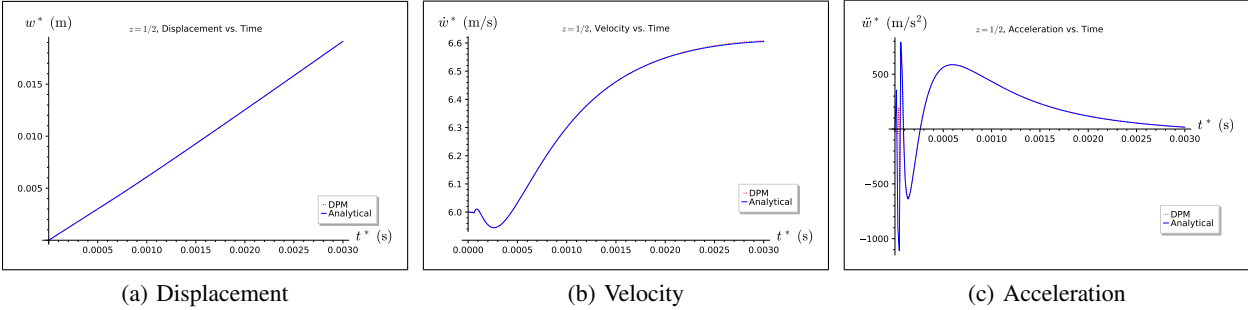


Figure 4.5.4:  $20'$ , empty: comparison of analytical model and DPM at  $z = 1/2$ .

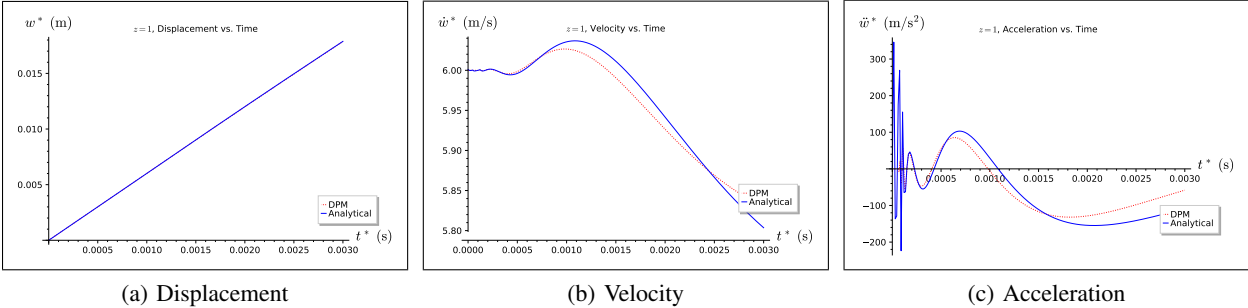


Figure 4.5.5:  $20'$ , empty: comparison of analytical model and DPM at  $z = 1$ .

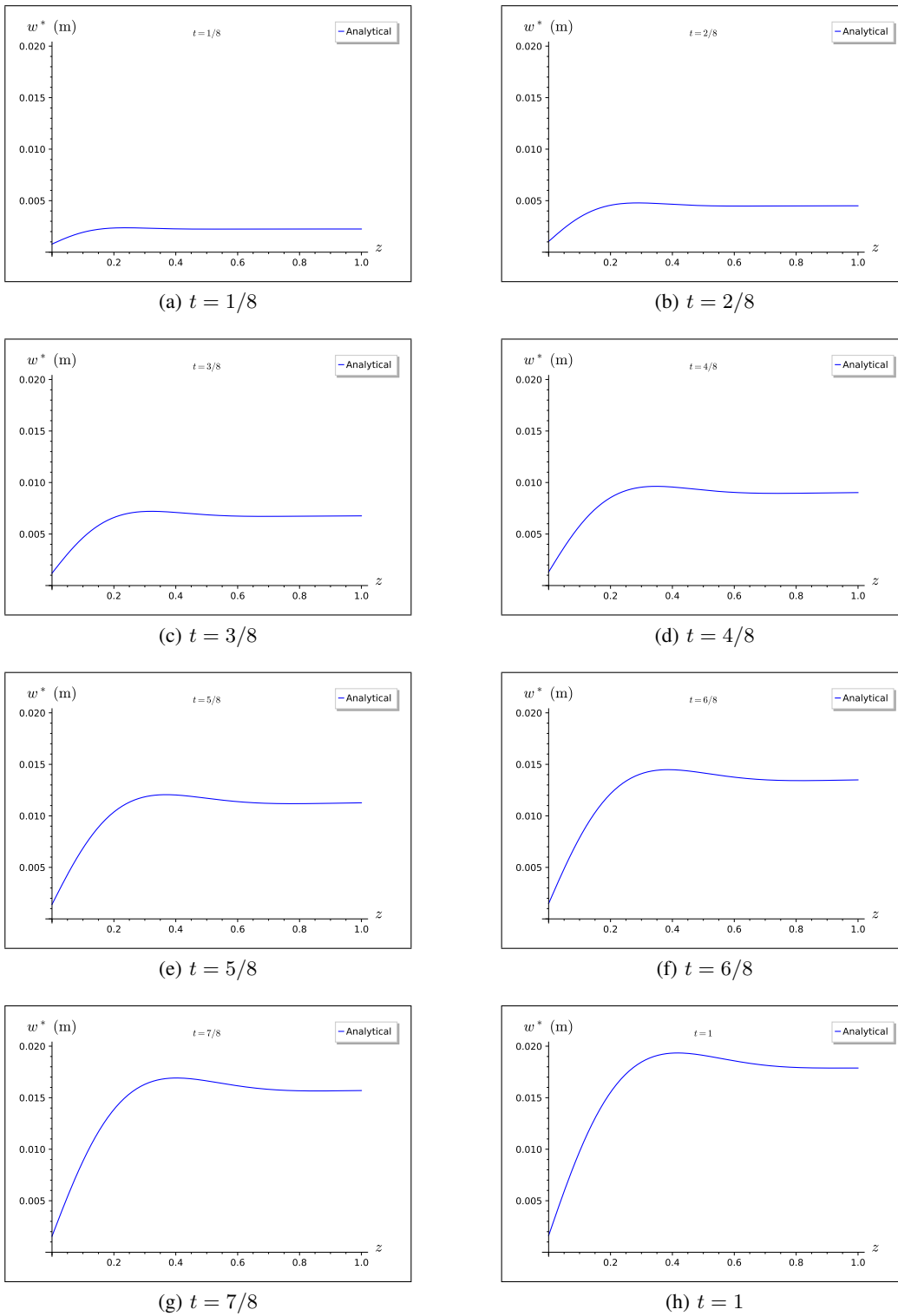
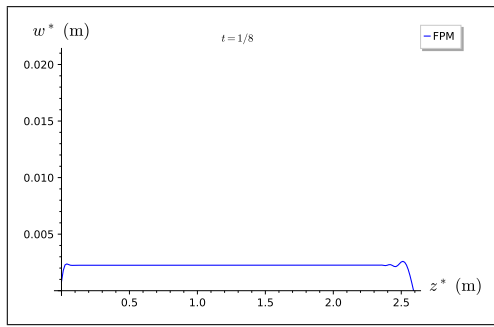
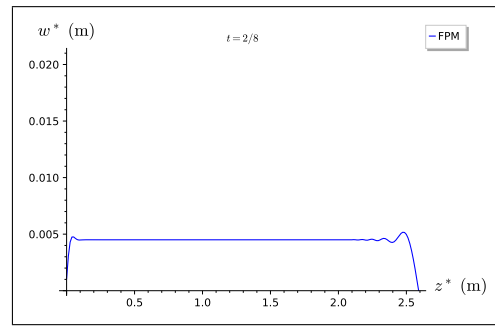


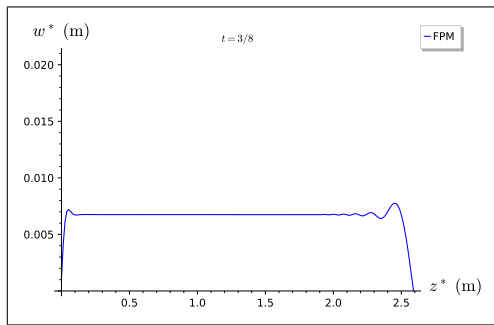
Figure 4.5.6: 20', empty: analytical 2-D displacement of the draft portion of the plate.



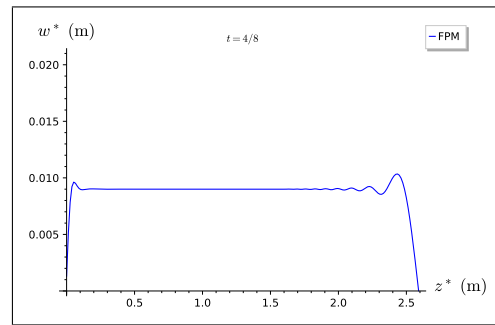
(a)  $t = 1/8$



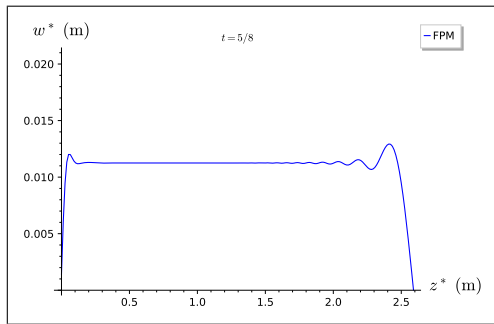
(b)  $t = 2/8$



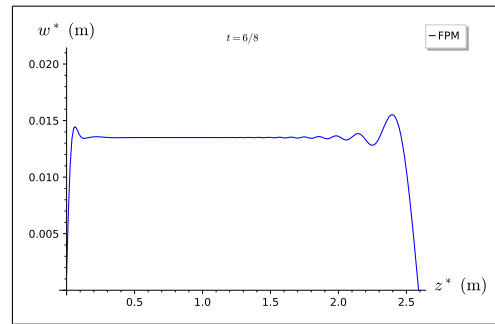
(c)  $t = 3/8$



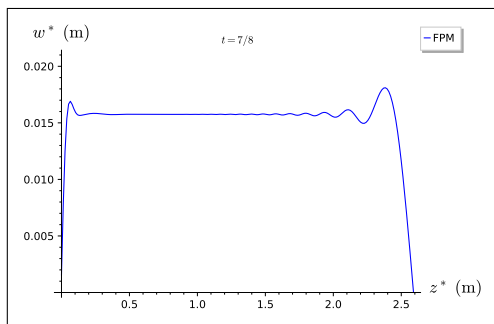
(d)  $t = 4/8$



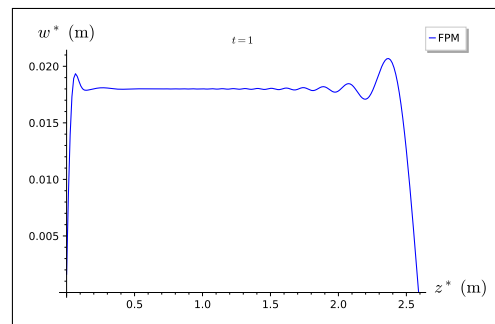
(e)  $t = 5/8$



(f)  $t = 6/8$

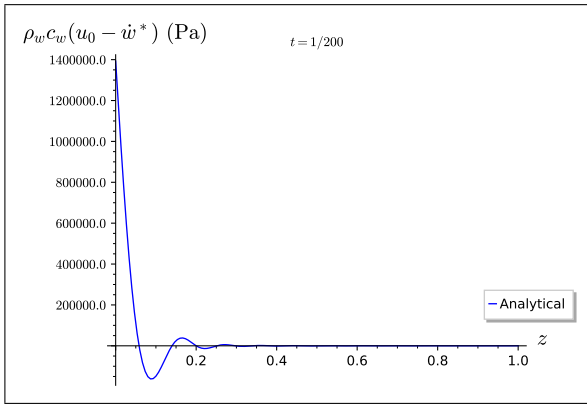


(g)  $t = 7/8$

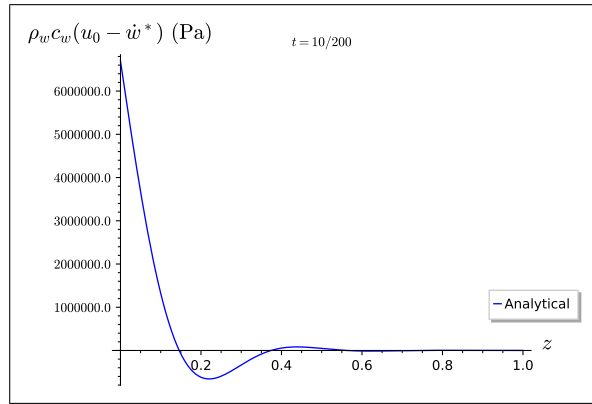


(h)  $t = 1$

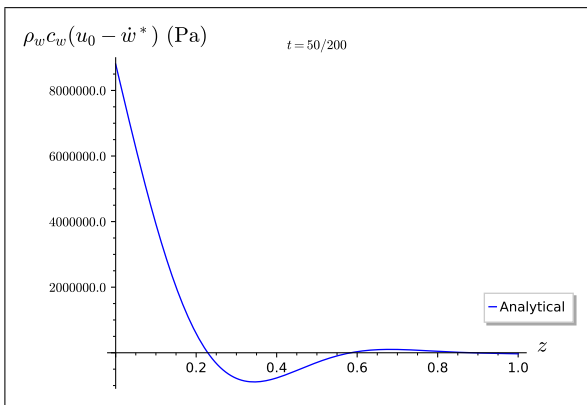
Figure 4.5.7: 20', empty: FPM 2-D displacement of the full plate.



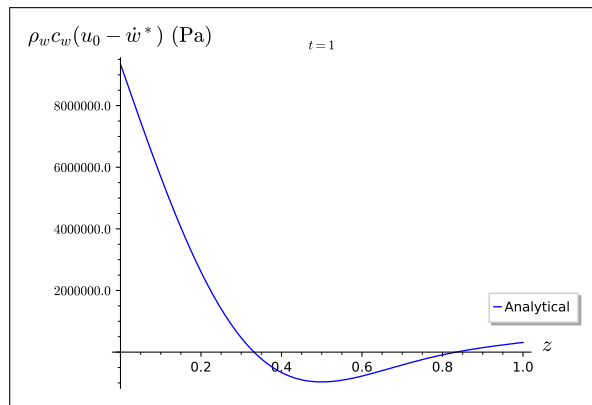
(a)  $t = 1/200$



(b)  $t = 10/200$



(c)  $t = 50/200$



(d)  $t = 1$

Figure 4.5.8:  $20^\circ$ , empty: relative acoustic load over the plate.

#### 4.6. 40-Foot Container at 100% Capacity

The 40-foot shipping container at maximum capacity is now considered. Its mass is  $m_{con} = 30,480$  kg, which yields a draft of  $L = 1.000$  m (about 39% of the full plate). This case used  $N = 140$  modes.

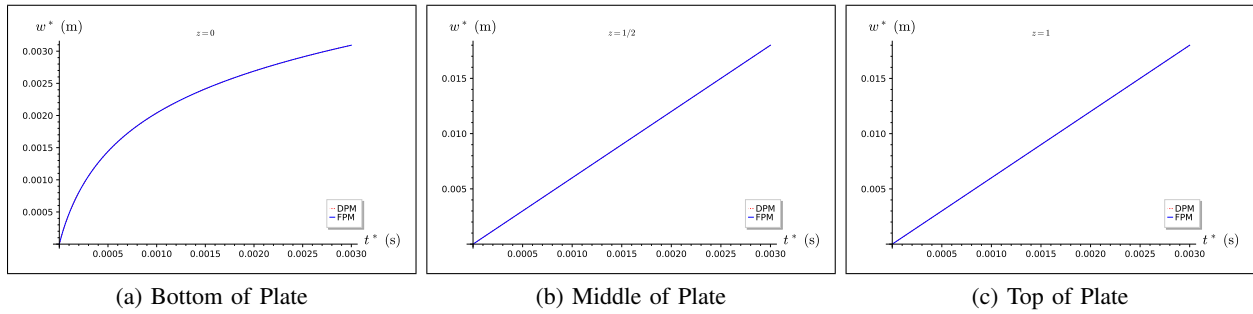


Figure 4.6.1: 40', 100%: displacement comparisons of finite element DPM and FPM.

Table 4.4: 40', 100%: analytical results.

$n$	$\beta_n$	$C_{1,n}$	$C_{3,n}$	$\dot{q}_n(0)$	$f_{t,n}$
1	1.5595	$1.8181 \times 10^5$	827.2	0.0068433	228.04
2	4.6791	6695.1	-5.1208	0.062281	2075.4
3	7.7993	1445.9	-0.93598	0.17302	5765.5
4	10.920	526.16	-1.0014	0.34003	11331
5	14.040	247.01	-0.99996	0.56448	18810

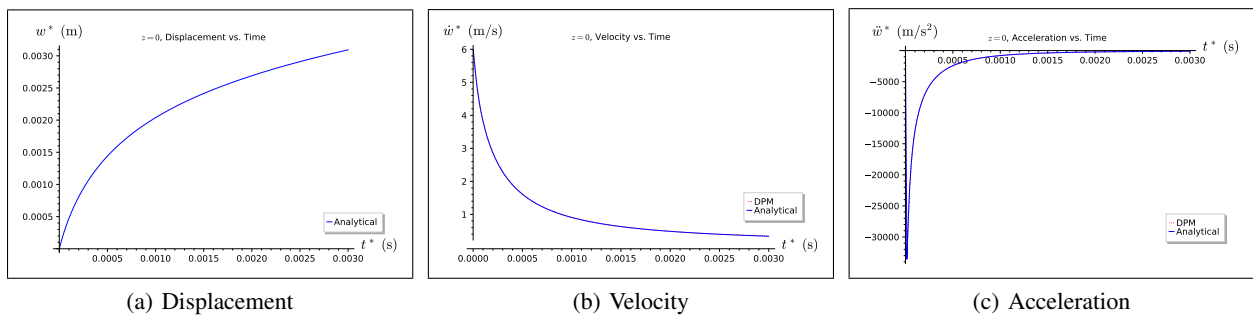


Figure 4.6.2: 40', 100%: comparison of analytical model and DPM at  $z = 0$ .

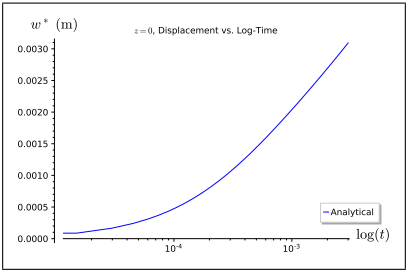


Figure 4.6.3: 40', 100%:  $z = 0$ , displacement vs. logarithm of time.

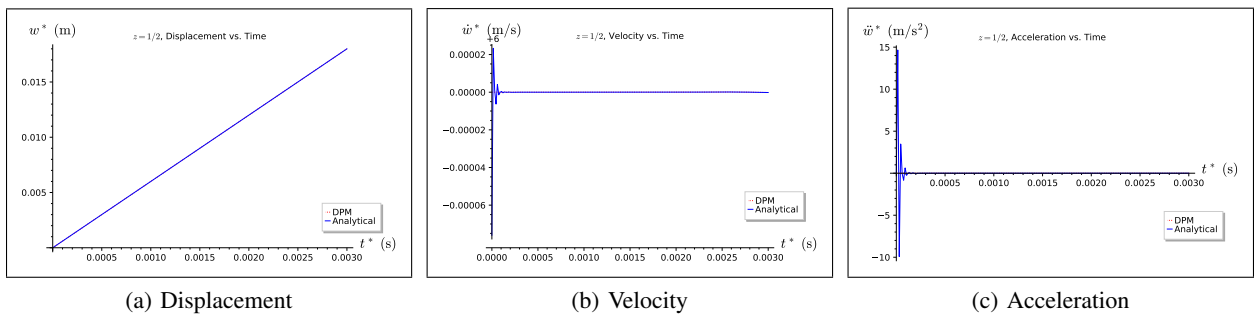


Figure 4.6.4: 40', 100%: comparison of analytical model and DPM at  $z = 1/2$ .

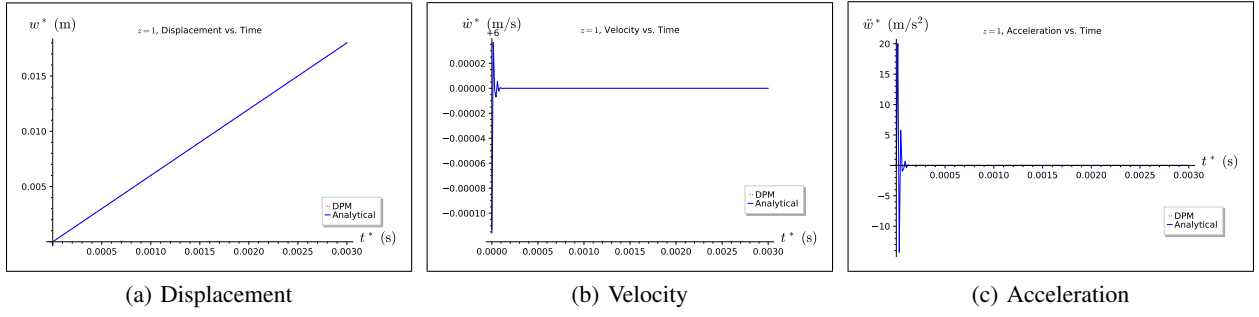
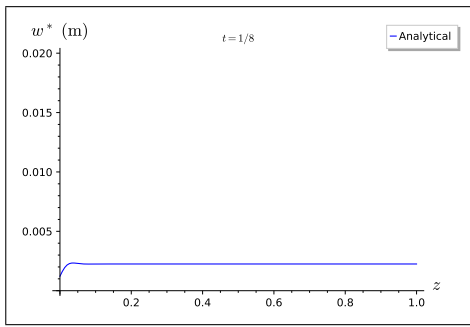
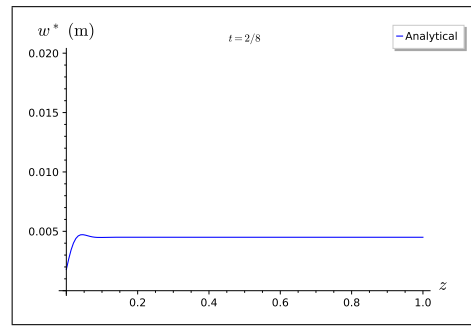


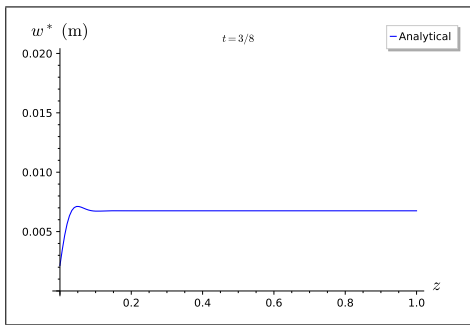
Figure 4.6.5: 40', 100%: comparison of analytical model and DPM at  $z = 1$ .



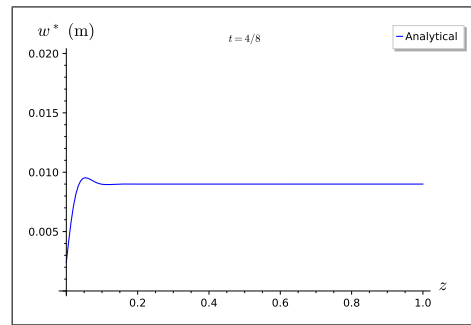
(a)  $t = 1/8$



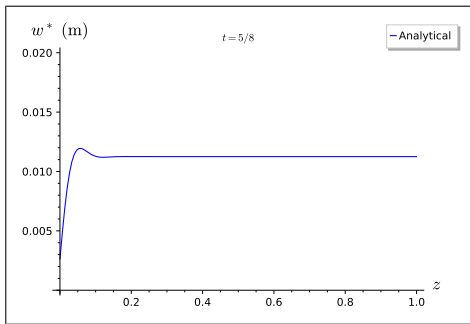
(b)  $t = 2/8$



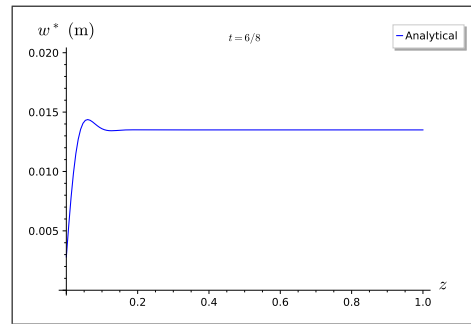
(c)  $t = 3/8$



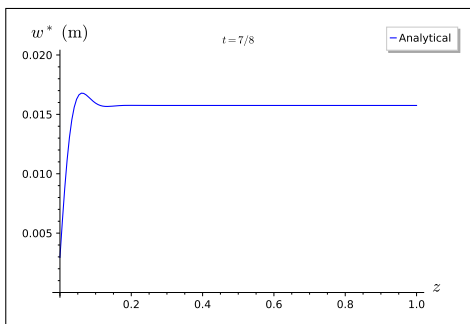
(d)  $t = 4/8$



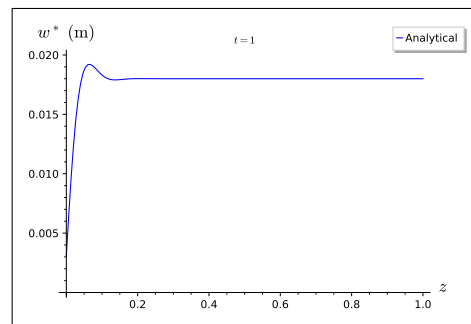
(e)  $t = 5/8$



(f)  $t = 6/8$

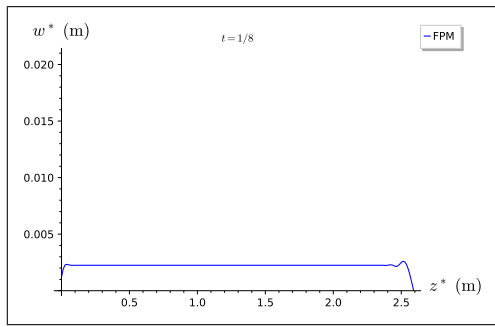


(g)  $t = 7/8$

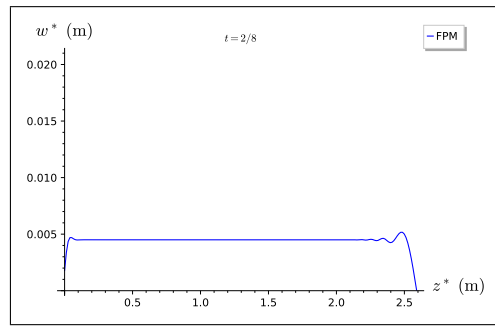


(h)  $t = 1$

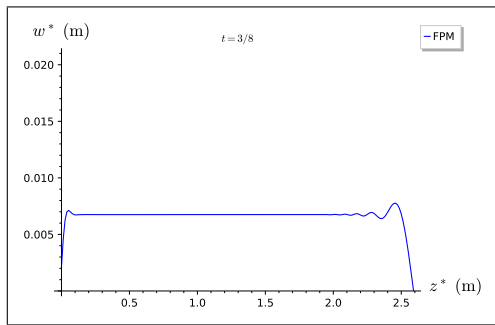
Figure 4.6.6:  $40^\circ$ , 100%: analytical 2-D displacement of the draft portion of the plate.



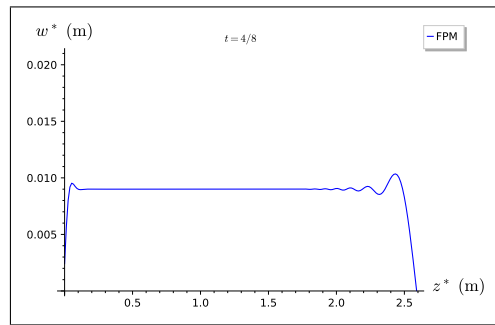
(a)  $t = 1/8$



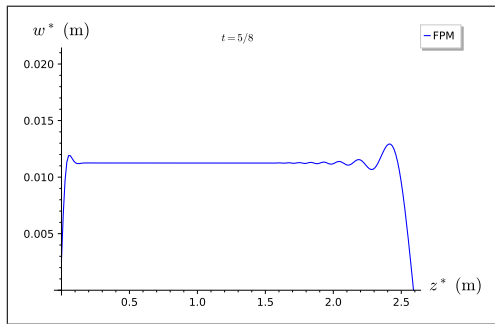
(b)  $t = 2/8$



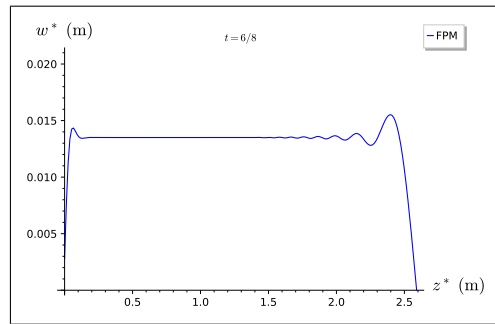
(c)  $t = 3/8$



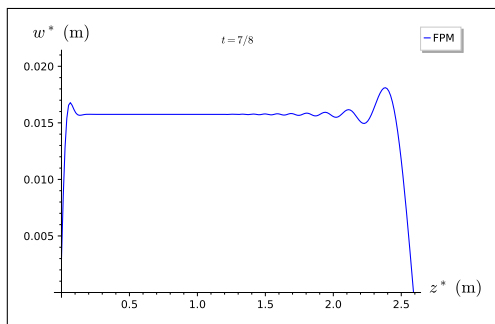
(d)  $t = 4/8$



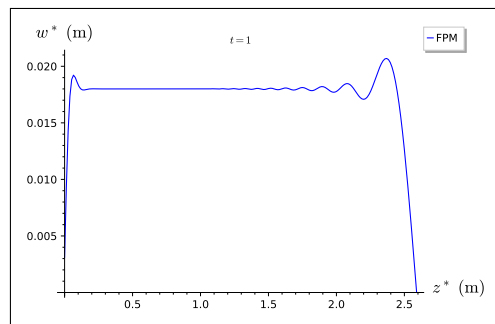
(e)  $t = 5/8$



(f)  $t = 6/8$

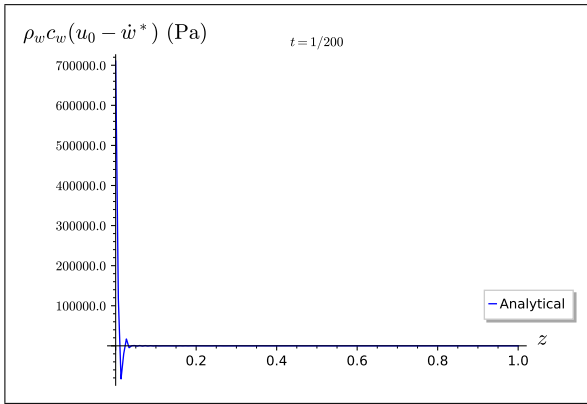


(g)  $t = 7/8$

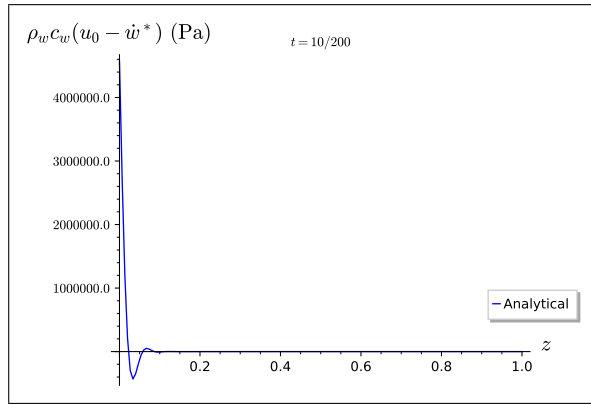


(h)  $t = 1$

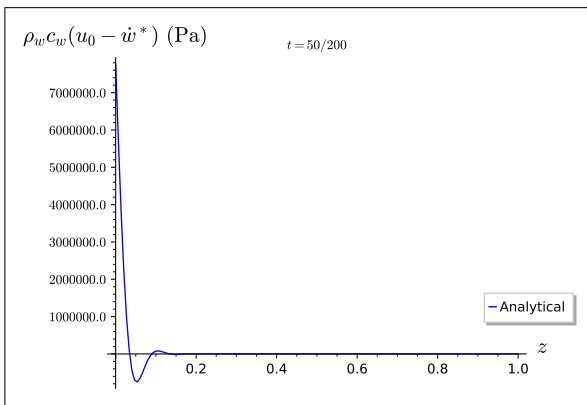
Figure 4.6.7: 40', 100%: FPM 2-D displacement of the full plate.



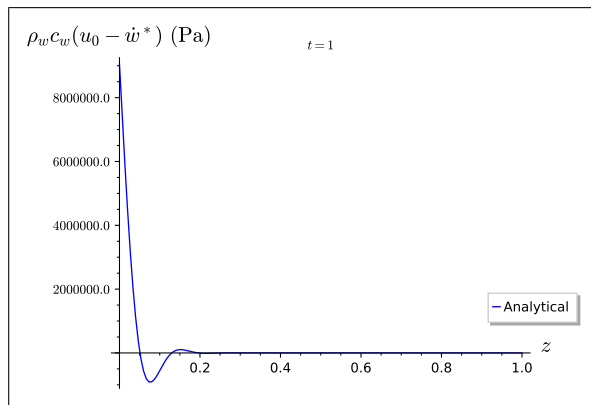
(a)  $t = 1/200$



(b)  $t = 10/200$



(c)  $t = 50/200$



(d)  $t = 1$

Figure 4.6.8: 40', 100%: relative acoustic load over the plate.

## 4.7. 40-Foot Container at 50% Capacity

The 40-foot shipping container at half capacity mass is now considered. Its mass is  $m_{con} = 17,230$  kg, which yields a draft of  $L = 0.565$  m (about 22% of the full plate). This case used  $N = 45$  modes.

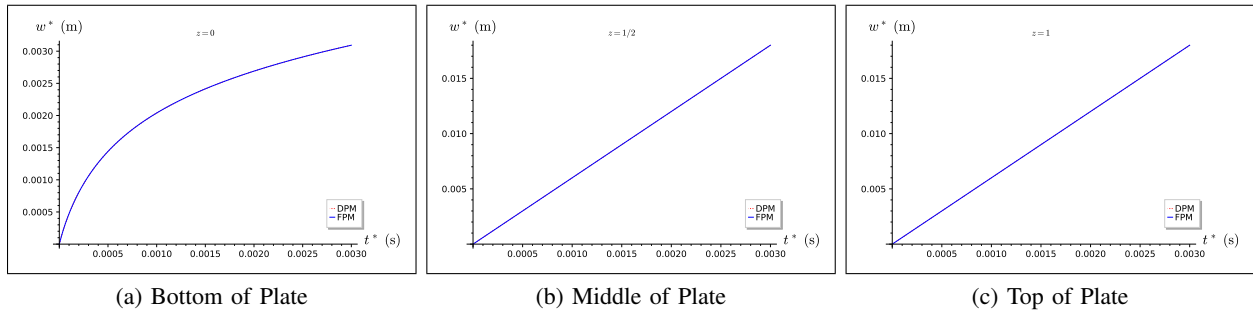


Figure 4.7.1: 40', 50%: displacement comparisons of finite element DPM and FPM.

Table 4.5: 40', 50%: analytical results.

$n$	$\beta_n$	$C_{1,n}$	$C_{3,n}$	$\dot{q}_n(0)$	$f_{t,n}$
1	1.5366	34658	485.44	0.011371	121.09
2	4.6161	1257.2	-3.3698	0.10636	1132.5
3	7.7013	270.49	-0.96368	0.29697	3162.3
4	10.790	97.714	-1.0008	0.59097	6292.9
5	13.878	45.386	-0.99998	1.0001	10649

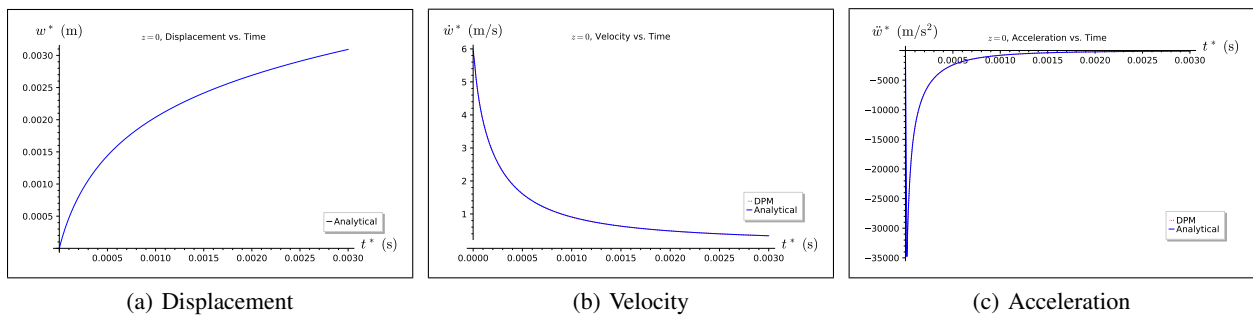


Figure 4.7.2: 40', 50%: comparison of analytical model and DPM at  $z = 0$ .

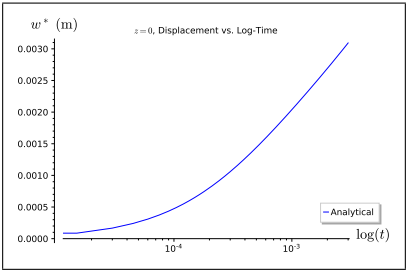


Figure 4.7.3: 40', 50%:  $z = 0$ , displacement vs. logarithm of time.

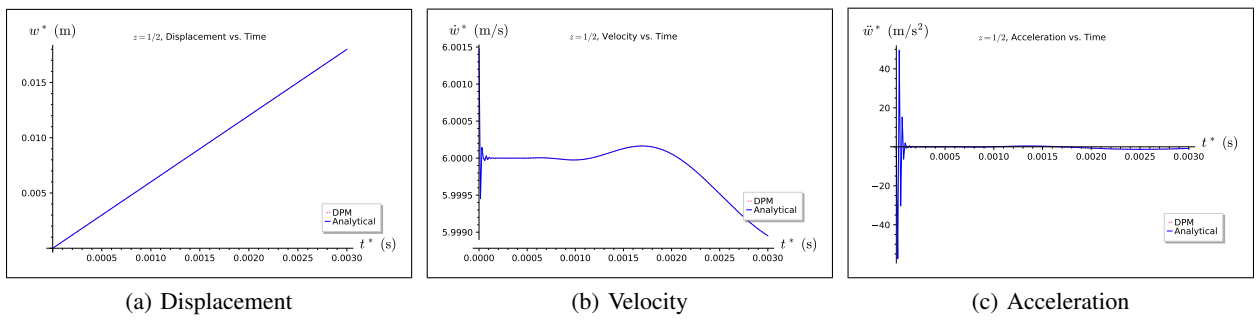


Figure 4.7.4: 40', 50%: comparison of analytical model and DPM at  $z = 1/2$ .

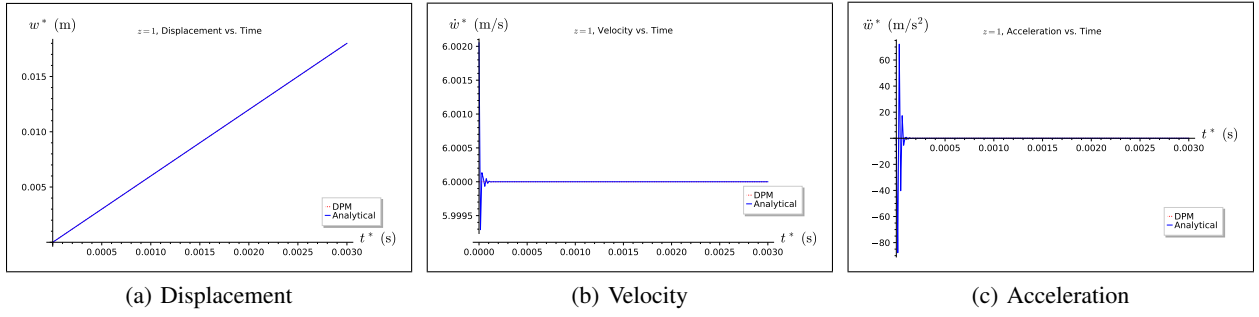
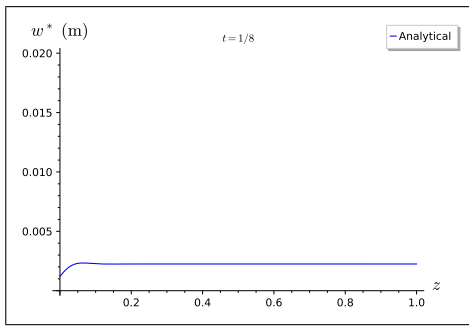
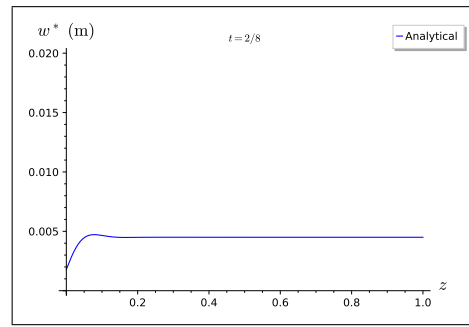


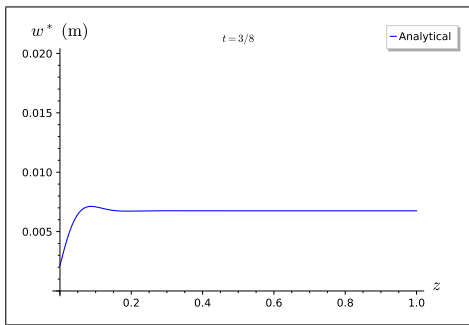
Figure 4.7.5: 40', 50%: comparison of analytical model and DPM at  $z = 1$ .



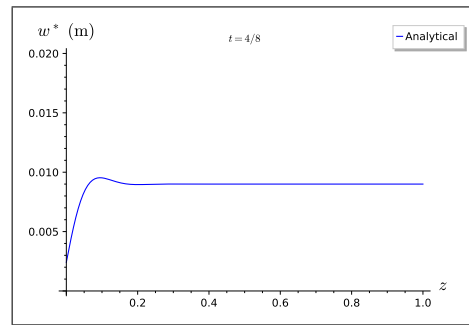
(a)  $t = 1/8$



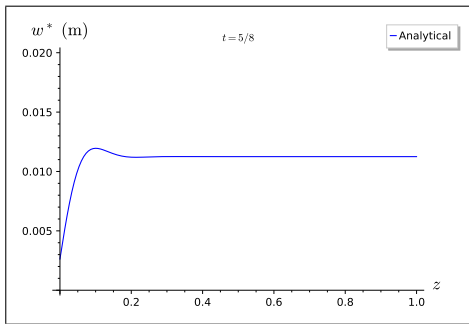
(b)  $t = 2/8$



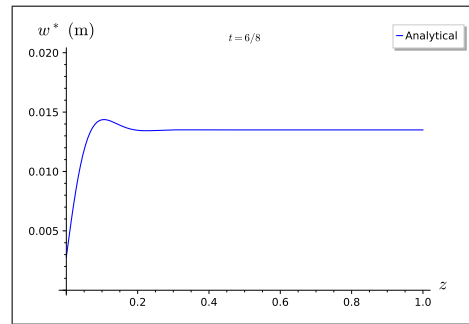
(c)  $t = 3/8$



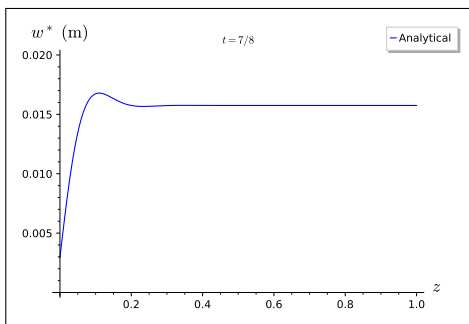
(d)  $t = 4/8$



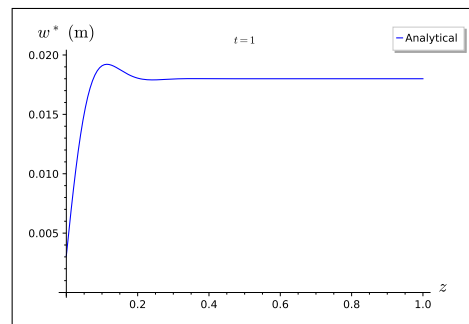
(e)  $t = 5/8$



(f)  $t = 6/8$

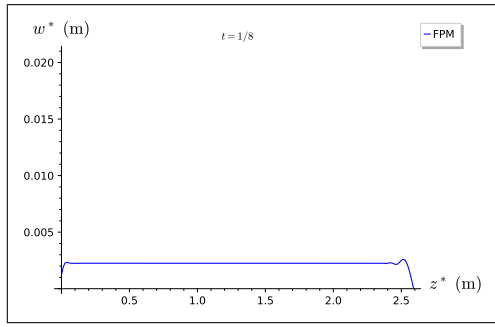


(g)  $t = 7/8$

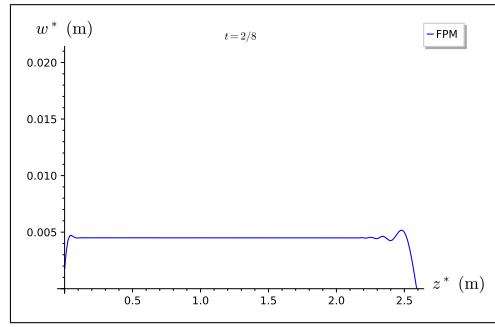


(h)  $t = 1$

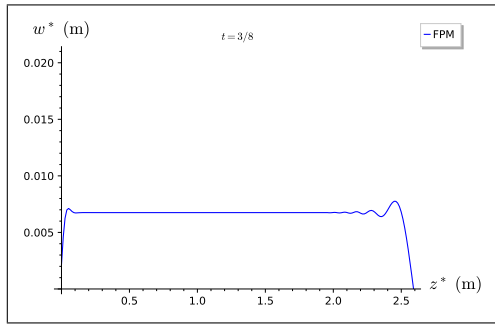
Figure 4.7.6: 40', 50%: analytical 2-D displacement of the draft portion of the plate.



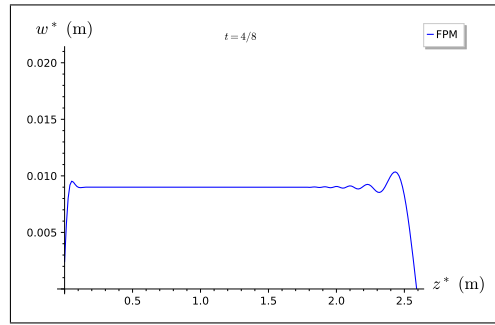
(a)  $t = 1/8$



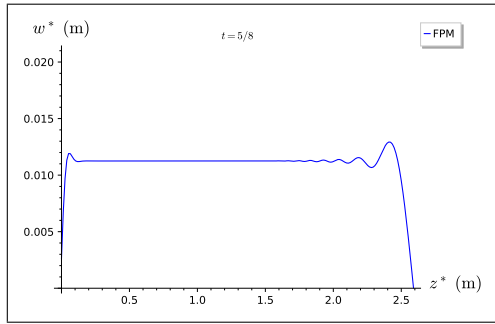
(b)  $t = 2/8$



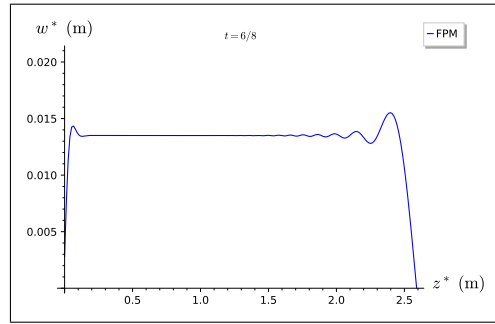
(c)  $t = 3/8$



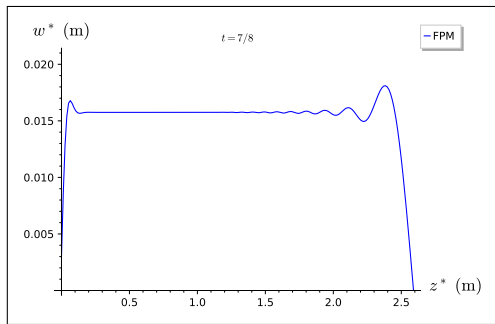
(d)  $t = 4/8$



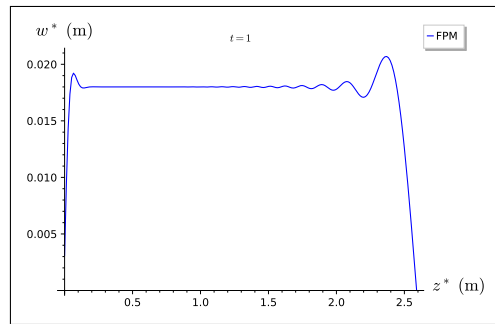
(e)  $t = 5/8$



(f)  $t = 6/8$

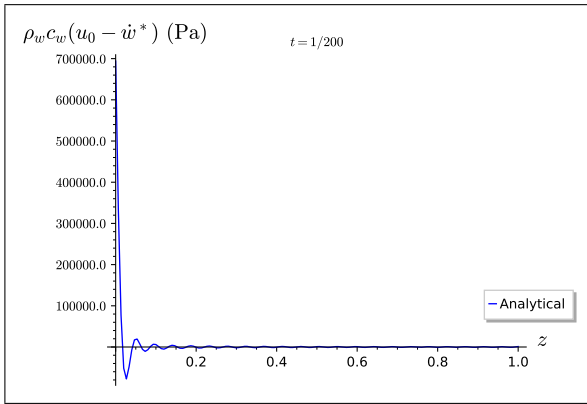


(g)  $t = 7/8$

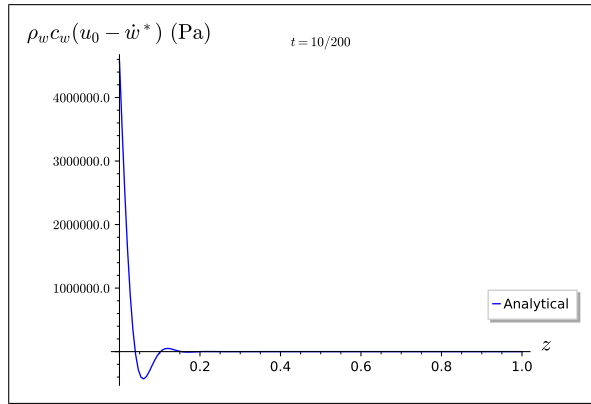


(h)  $t = 1$

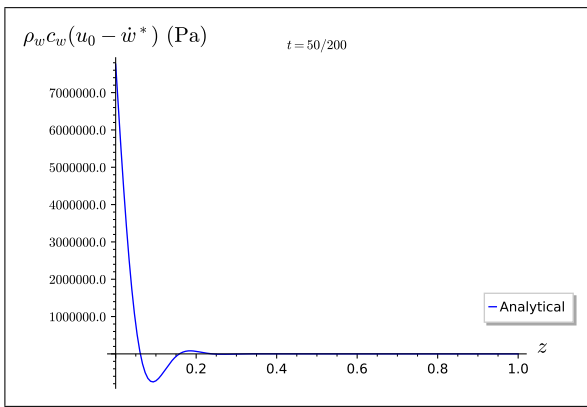
Figure 4.7.7:  $40^\circ$ , 50%: FPM 2-D displacement of the full plate.



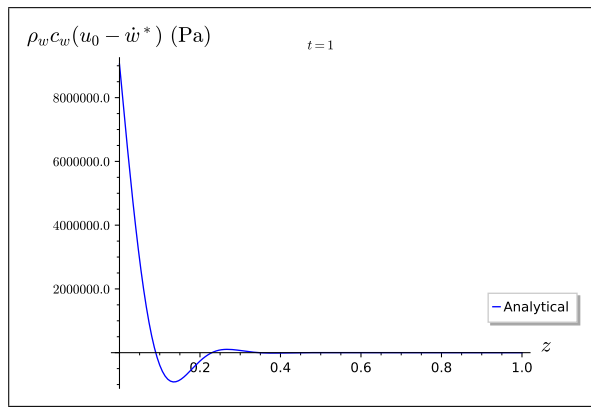
(a)  $t = 1/200$



(b)  $t = 10/200$



(c)  $t = 50/200$



(d)  $t = 1$

Figure 4.7.8: 40', 50%: relative acoustic load over the plate.

## 4.8. 40-Foot Container Empty

The empty 40-foot shipping container is now considered. Its mass is  $m_{con} = 3,980$  kg, which yields a draft of  $L = 0.131$  m (about 5% of the full plate). This case used  $N = 25$  modes.

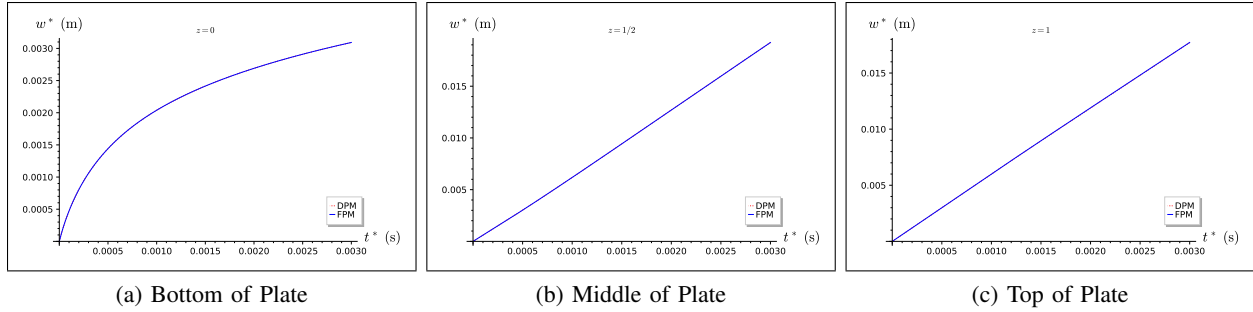


Figure 4.8.1: 40', empty: displacement comparisons of finite element DPM and FPM.

Table 4.6: 40', empty: analytical results.

$n$	$\beta_n$	$C_{1,n}$	$C_{3,n}$	$\dot{q}_n(0)$	$f_{t,n}$
1	1.2207	1030.6	190.52	0.018851	10.711
2	4.0958	20.868	-1.3739	0.3872	220
3	6.9390	3.5783	-0.99568	1.3764	782.05
4	9.4350	0.81936	-1.0001	2.8477	1618
5	11.801	-0.070013	-0.99999	2.1133	1200.7

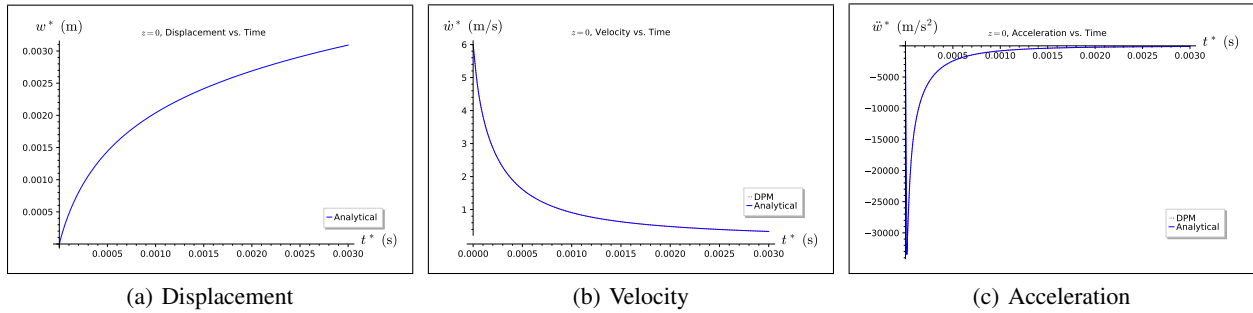


Figure 4.8.2: 40', empty: comparison of analytical model and DPM at  $z = 0$ .

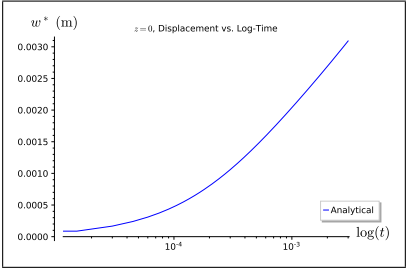


Figure 4.8.3: 40', empty:  $z = 0$ , displacement vs. logarithm of time.

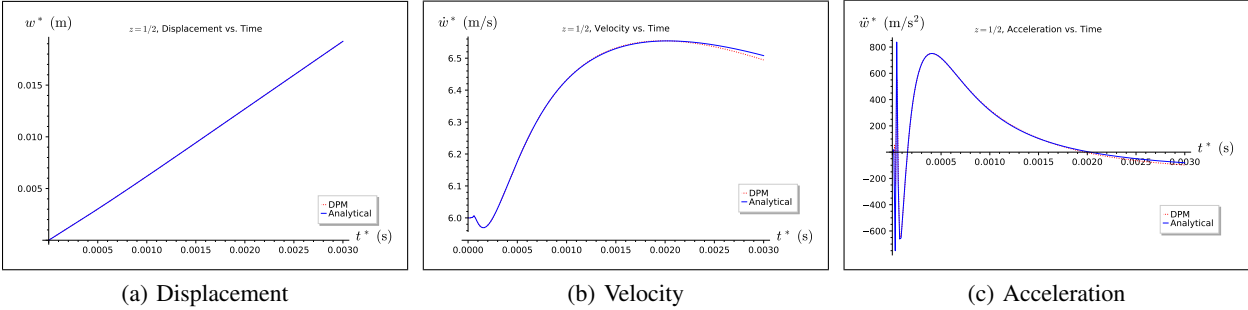


Figure 4.8.4: 40', empty: comparison of analytical model and DPM at  $z = 1/2$ .

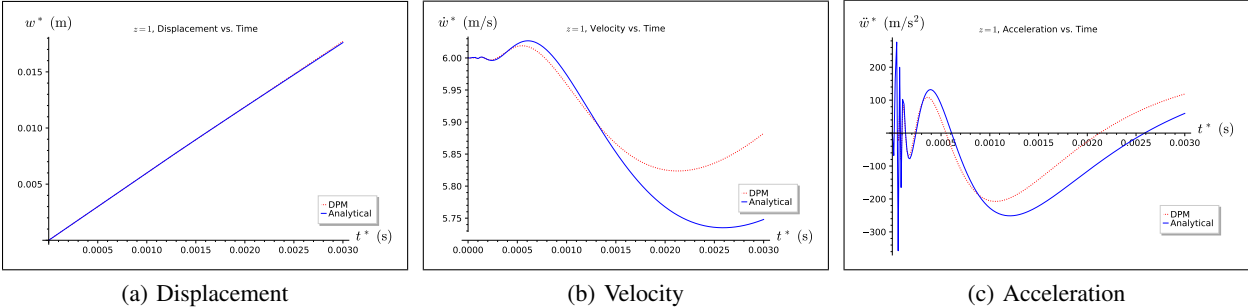


Figure 4.8.5: 40', empty: comparison of analytical model and DPM at  $z = 1$ .

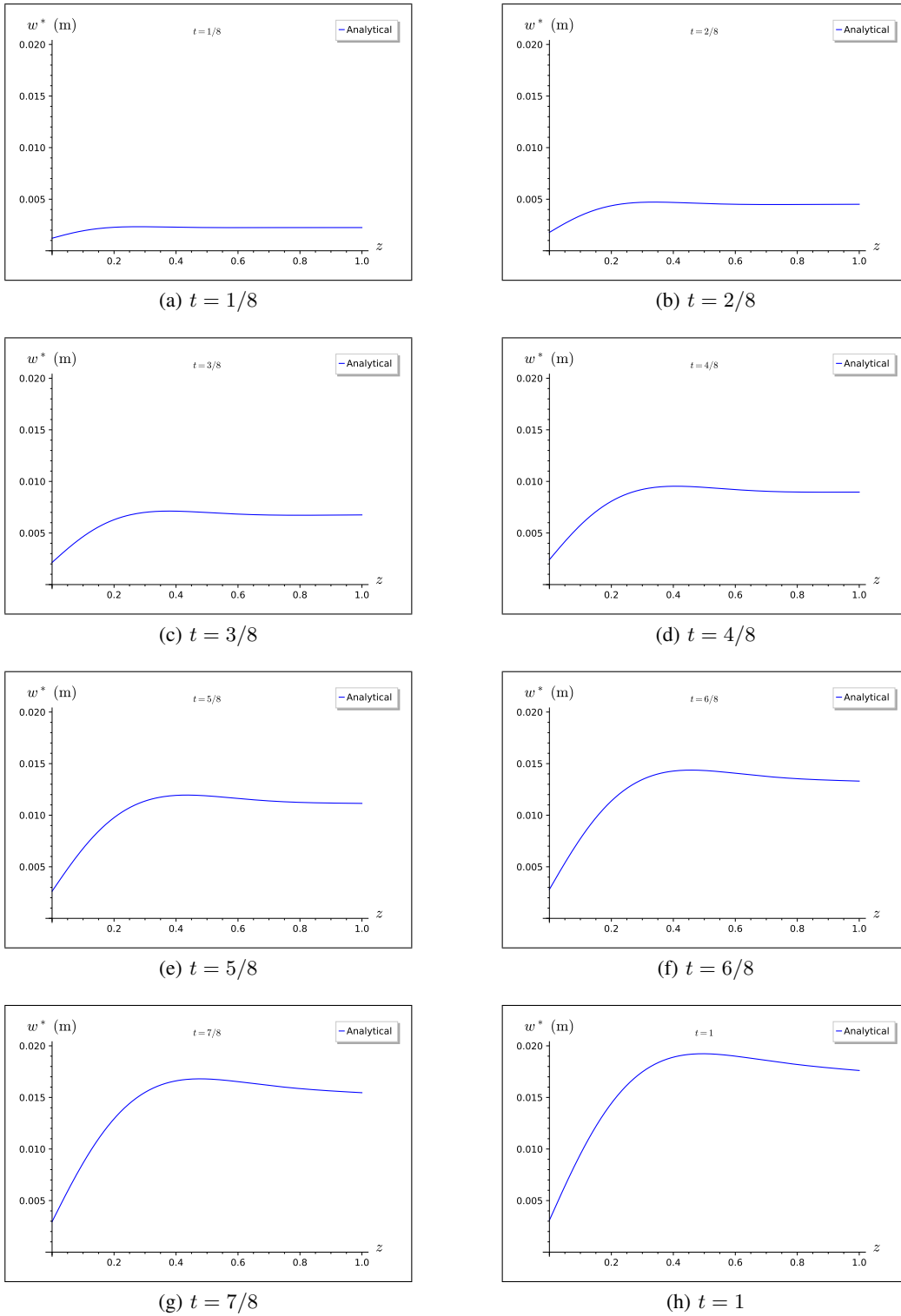
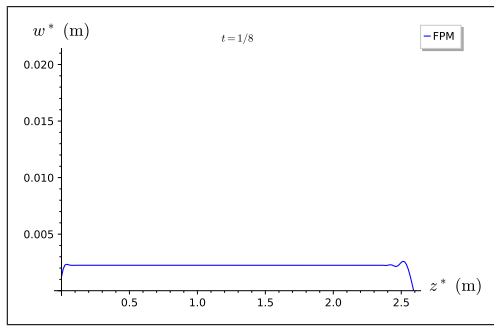
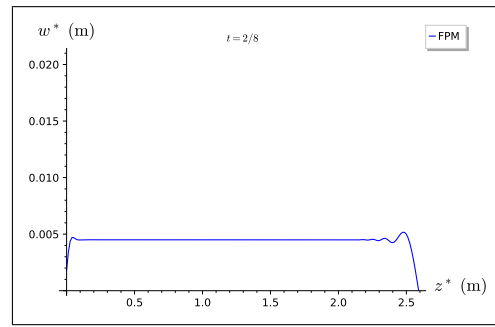


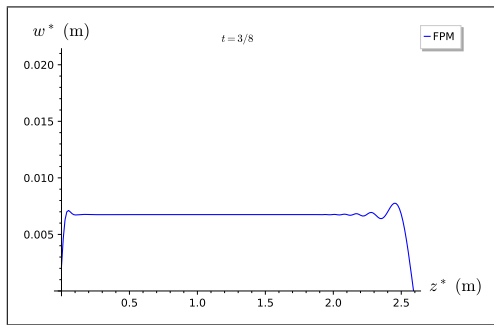
Figure 4.8.6: 40', empty: analytical 2-D displacement of the draft portion of the plate.



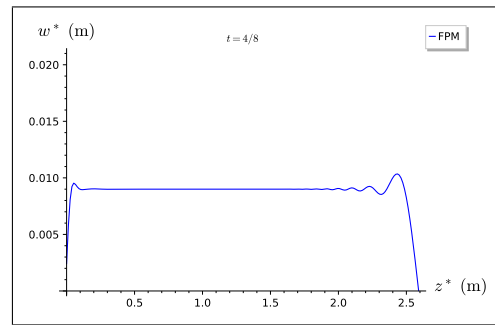
(a)  $t = 1/8$



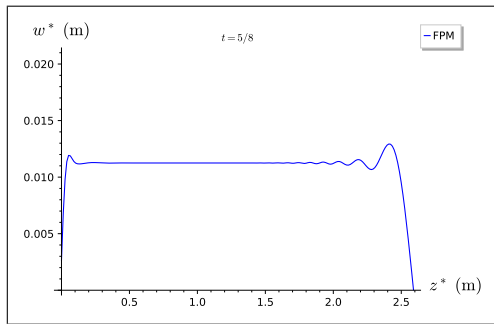
(b)  $t = 2/8$



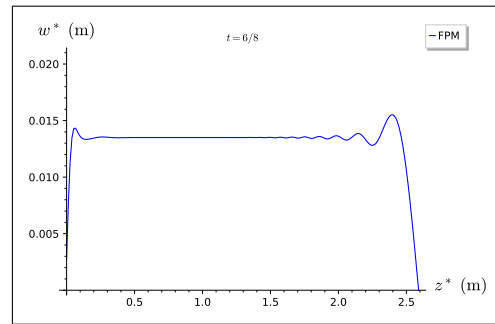
(c)  $t = 3/8$



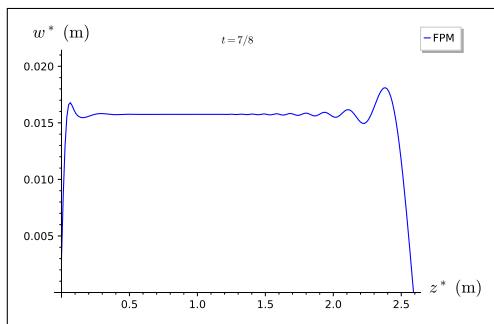
(d)  $t = 4/8$



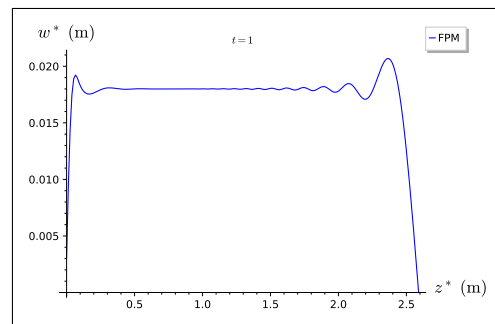
(e)  $t = 5/8$



(f)  $t = 6/8$

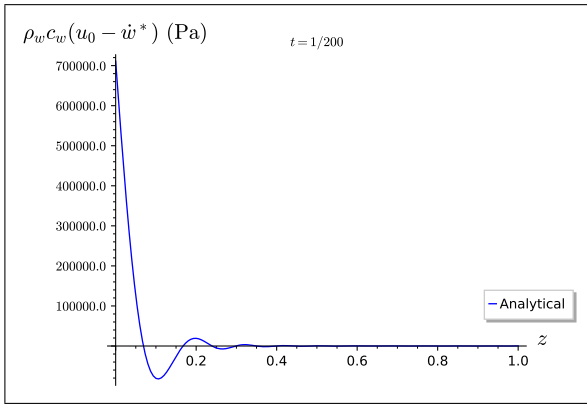


(g)  $t = 7/8$

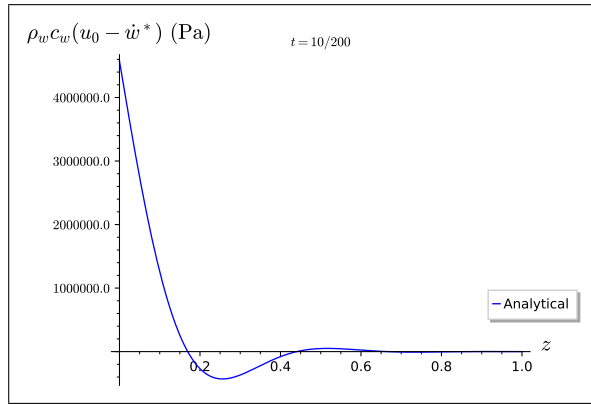


(h)  $t = 1$

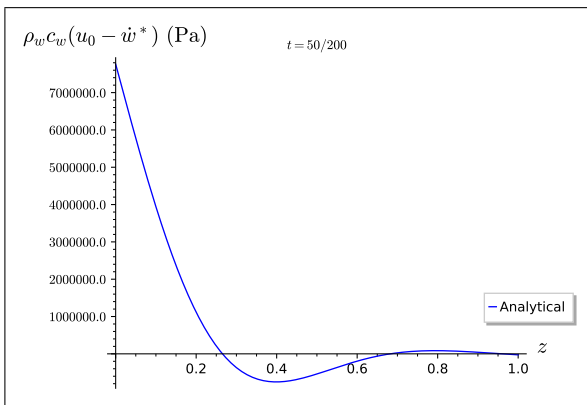
Figure 4.8.7: 40', empty: FPM 2-D displacement of the full plate.



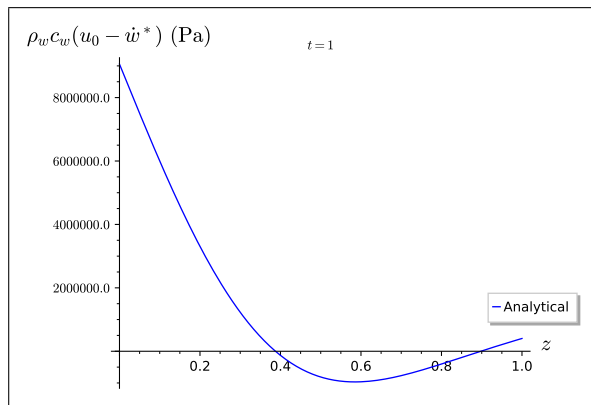
(a)  $t = 1/200$



(b)  $t = 10/200$



(c)  $t = 50/200$



(d)  $t = 1$

Figure 4.8.8:  $40^\circ$ , empty: relative acoustic load over the plate.

## 4.9. Discussion of the Results

In all six cases, visual agreement between the DPM and FPM was found when  $k_2^* = 0$  and  $k_t^* = 10^4$  N·m/rad. This shows that, because the plate is very thin, the rigidity of the upper, non-draft portion of the plate has very little effect on the draft portion. Since the values of the fictitious springs  $k_2^*$  and  $k_t^*$  are the same for all cases, reducing the mass of cargo in the container, and thus reducing the draft depth, has the effect of visually “zooming in” closer to  $z = 0$  on the graphs. Therefore, differences between the cases are mainly seen only when comparing the two different sizes of shipping containers. Indeed, the twice-as-long 40-foot container provides half the stiffness  $k_1^*$  of the 20-foot container, resulting in twice the displacement at  $z = 0$  in the cases of the longer container. The logarithmic time scale graphs show that the displacement at  $z = 0$  becomes logarithmic after roughly half a millisecond.

The agreement between the analytical model and DPM is very tight at  $z = 0$ , to the point where the plotted lines precisely overlap visually. At  $z = 1/2$  and  $z = 1$ , the displacements mostly agree very closely, but in the two empty container cases, the velocity and acceleration graphs agree to a lesser extent. Starting not much above  $z = 0$ , the velocity is nearly constant at the initial velocity, so any apparent lack of agreement in the graphs is actually not so stark, at least over the given time scale. Increasing the number of modes in the analytical model or increasing the number of elements or time steps in the DPM does not help the agreement. It is therefore likely that numerical dispersion due to the interpolation functions in the finite element model is to blame. Possible remedies may include finite elements with reduced dispersion [7, 8], or methods involving higher-order polynomials [24, 26].

Related to the constant velocity above  $z = 0$  is the fact that most of the plate above  $z = 0$  experiences roughly zero relative acoustic load. Therefore, most of the plate is not being pushed by the water, but rather it is moving with the water. The displacement and velocity graphs suggest that most of the plate above  $z = 0$  will likely continue to be displaced beyond any acoustic timescale.

The springs representing the bottom and top sides of the shipping container are rather soft, such that no recoil occurs with this acoustic timescale, not even at  $z = 0$ . In the draft-portion displacement graphs, a transverse wave can be seen forming above  $z = 0$ , but is damped out after one peak by the acoustic load. According to the relative acoustic load graphs, this portion of the plate outruns the water, yielding an erroneous negative acoustic load, which is a shortcoming of this model. In the FPM displacement graphs, a similar transverse wave can be seen above the draft portion of the plate. Above  $z = 0$ , a slight increase in the velocity above the initial velocity can be seen due to the sudden transverse

wave in the plate at impact. This is why the acoustic load drops to negative values, that is, the value of  $u_0 - \dot{w}$  is negative. Therefore, the acoustic load is really zero at this time, since the plate has momentarily outrun the water. Since it appears in both the analytical and numerical models, this phenomenon is likely due to the lack of shear deformation in Kirchhoff-Love plate theory. Although the plate is very thin, shear may be dominant over a small length close to the springs. Research involving beam impacts has found that shear is dominant at the time of impact [9, 10], requiring Timoshenko beam theory, and thus Mindlin-Reissner plate theory may be necessary to rectify this issue.

Related research found that non-rigidly attached, nonstructural mass does not affect the peak impact force of debris on structures [1, 11]. Similarly, the results herein show no significant difference in displacement when changing the draft depth due to the total mass of the container, which additionally agrees with research showing that the water has little effect on the impact beyond carrying the debris [11]. Also in agreement with related research is that the bulk of the deformation at  $z = 0$  occurs within the acoustic time scale of the water [12]. The graphs of the relative acoustic load show that at and around  $z = 0$  is by far the most important region to consider in terms of the load on the container shortly after impact.

# Chapter 5

## Conclusions and Future Work

### 5.1. Conclusions

An analytical model of the draft portion of the water-impacted panel of a shipping container was presented. The shipping container, carried by water modeled as an acoustic load, is assumed to have impacted a rigid structure. The acoustic load provides a conservative upper bound of the pressure of the water on the container. The water-impacted panel was modeled as a Kirchhoff-Love plate, which describes the displacement of this portion of the container. The model was validated using finite element models for the six cases of a 20-foot and 40-foot shipping container, each at 100%, 50%, or zero cargo capacity. However, the acoustic load on the water-impacted panel was not accurately modeled where the model yields negative values of the load.

It was found that varying the mass of the cargo in the shipping container made no significant difference in the results, and only that changing the debris length made a difference due to the stiffness of the bottom side of the container. This is also the region where the acoustic load is by far the most significant, whereas the rest of the water-impacted panel experiences steady displacement, continuing with the constant velocity of the water. Agreement was found with related research in that the mass of the shipping container made no significant difference in the results, that the water has little effect on the container beyond carrying it, and that most of the deformation of the important bottom area occurs within the acoustic time scale of the water.

### 5.2. Future Work

#### Use of Three-Dimensional Plate Theory

In addition to lower and upper panels already modeled, the real water-impacted panel of the shipping container is connected to the left and right side panels of the container, whose stiffnesses were neglected. Therefore, the real water-impacted panel may exhibit significantly three-dimensional deformation, deforming more around the center, while deforming less near the four connected panels.

Since this study showed that the acoustic load is significant only around the bottom side of the container, it stands to reason that some additional load would be experienced by the water-impacted panel on the left and right sides. The larger the draft portion is, the larger the total force on the container would be, which was not the case in this study.

### **Inclusion of the Impacted Structure**

Since the broader purpose of this and related studies is to understand the forces on debris-impacted structures, a representation of a structure could be added to the given 2-dimensional model at the right side of the springs  $k_1$  and  $k_3$ . The force due to the acoustic load would be propagated to the structure through the springs. The structure could be a rigid wall with or without a contact stiffness, as in the analytical model presented in [12], or another plate, which would model the deformation of the impacted face of the structure.

## References

- [1] Aghl, P. Piran, C. J. Naito, and H. R. Riggs. "Effect of nonstructural mass on debris impact demands: Experimental and simulation studies." *Engineering Structures*. 88 (2015): 163-175.
- [2] Aghl, P. Piran, C. J. Naito, and H. R. Riggs. "Estimation of demands resulting from inelastic axial impact of steel debris." *Engineering Structures*. 82 (2015): 11-21.
- [3] Aghl, P. Piran, C. J. Naito, and H. R. Riggs. "Study of demands resulting from transverse impact of high mass, low velocity debris." *Advances in Structural Engineering*. Vol. 19(8) 1328-1344, 2016.
- [4] Container Alliance 20-foot shipping container overview.  
<[https://ca-containeralliance.com/containers/sales/wind-and-water-tight/20ft#/>](https://ca-containeralliance.com/containers/sales/wind-and-water-tight/20ft#/)
- [5] Eaton, John W., David Bateman, Søren Hauberg, Rik Wehbring. GNU Octave version 6.2.0 manual: a high-level interactive language for numerical computations. <https://docs.octave.org/v6.2.0/>. 2021.
- [6] Ferreira, Antonio J. M., and Nicholas Fantuzzi. *MATLAB Codes for Finite Element Analysis: Solids and Structures*. 2nd ed. Cham, Switzerland: Springer Nature.
- [7] Idesman, A. V., M. Schmidt, and J. R. Foley. "Accurate finite element modeling of linear elastodynamics problems with the reduced dispersion error." *Computational Mechanics*. (2011) 47:555–572.
- [8] Idesman, A. V. "Finite element modeling of linear elastodynamics problems with explicit time-integration methods and linear elements with reduced dispersion. Comparative study of different finite element techniques used for elastodynamics." 4th ECCOMAS Thematic Conference on Computational Methods in Structural Dynamics and Earthquake Engineering. June 2013, 759-776.
- [9] Khowitar, Eid, H. R. Riggs, and Marcelo H. Kobayashi. "Beam Response to Longitudinal Impact by a Pole." *Journal of Engineering Mechanics*. 2014, 140(7), 04014045.
- [10] Khowitar, Eid, H. R. Riggs, and Marcelo H. Kobayashi. "Transverse Impact of a Horizontal Beam on a Vertical Column." *Journal of Engineering Mechanics*. 2016, 142(2), 04015085.
- [11] Ko, H. T.-S., D. T. Cox, H. R. Riggs, and C. J. Naito. "Hydraulic Experiments on Impact Forces from Tsunami-Driven Debris." *Journal of Waterway, Port, Coastal, and Ocean Engineering*. 2015, 141(3): 04014043.
- [12] Kobayashi, Marcelo H., R. Genest, H. Ronald Riggs, and K. Paczkowski. "Simple hydroelastic impact models for waterborne debris." *Journal of Engineering for the Maritime Environment*. 226.170 (2012): 170-179.
- [13] Kwon, Young W., and Hyochoong Bang. *The Finite Element Method Using MATLAB*. 3rd ed. Boca Raton, FL: CRC Press, 2000.
- [14] Leissa, Arthur W., and Mohamad S. Qatu. *Vibrations of Continuous Systems*. New York: The McGraw-Hill Companies, Inc., 2011.

- [15] Magrab, Edward B. *Vibrations of Elastic Systems: With Applications to MEMS and NEMS*. Dordrecht: Springer, 2012.
- [16] Naito, Clay, H. R. Riggs, Yong Wei, and Christina Cercone. "Shipping-Container Impact Assessment for Tsunamis." *Journal of Waterway, Port, Coastal, and Ocean Engineering*. 2016, 142(5): 05016003.
- [17] Paczkowski, Krystian, H. Ronald Riggs, and Ian N. Robertson. "Bore impact upon vertical wall and water-driven, high-mass, low-velocity debris impact." Research report, University of Hawai'i at Mānoa.  
<<http://www.cce.hawaii.edu/wp-content/uploads/UHM-CEE-11-05.pdf>>
- [18] Pickford, John. *Analysis of Water Surge*. New York: Gordon and Breach Science Publishers, Inc., 1969.
- [19] Rao, Singiresu S. *Vibration of Continuous Systems*. 2nd ed. Hoboken, NJ: John Wiley & Sons, Inc., 2019.
- [20] Reddy, J. N. *An Introduction to the Finite Element Method*. 3rd ed. Boston, MA: McGraw-Hill, 2006.
- [21] Reddy, J. N. *Theory and Analysis of Elastic Plates and Shells*. 2nd ed. Boca Raton, FL: CRC Press, 2007.
- [22] "Standard gauge for sheet and plate iron and steel." Legal Information Institute, Cornell University Law School.  
<<https://www.law.cornell.edu/uscode/text/15/206>>
- [23] The Sage Developers. *SageMath, the Sage Mathematics Software System*. Version 9.6. <https://www.sagemath.org>.
- [24] Scott, Waymond R., Jr. "Numerical dispersion in the finite element method." Proceedings of IEEE Antennas and Propagation Society International Symposium and URSI National Radio Science Meeting. June 1994, 2080-2083.
- [25] Spiegel, Murray R. *Applied Differential Equations*. 3rd ed. Englewood Cliffs, NJ: Printice-Hall, Inc., 1981.
- [26] Thompson, Lonny, L. "A review of finite element methods for time-harmonic acoustics." *The Journal of the Acoustical Society of America*. 119(3), 1315–1330 (2006).
- [27] Thorley, A. R. David. *Fluid Transients in Pipeline Systems*. 2nd ed. New York: ASME Press, 2004.
- [28] TransMed Logistics s.a.r.l. *Sea Container Sizes*. [https://www.transmedlogistics.com/pdf/sea\\_container-Sizes.pdf](https://www.transmedlogistics.com/pdf/sea_container-Sizes.pdf).
- [29] Wang, C. M., J. N. Reddy, and K. H. Lee. *Shear Deformable Beams and Plates: Relationships with Classical Solutions*. Oxford, UK: Elsevier Science Ltd., 2000.
- [30] Young, Warren C., and Richard G. Budynas. *Roark's Formulas for Stress and Strain*. 7th ed. New York: The McGraw-Hill Companies Inc., 2002.
- [31] Young, Dana, and Robert P. Flegar, Jr. *Table of characteristic functions representing normal modes of vibration of a beam*. The University of Texas at Austin publication No. 4913, July 1, 1949.  
<<https://repositories.lib.utexas.edu/bitstream/handle/2152/6001/young.pdf?sequence=2>>
- [32] Zienkiewicz, O. C., R. L. Taylor, and J. Z. Zhu. *The Finite Element Method: Its Basis and Fundamentals*. 7th ed. Oxford, UK: Elsevier Ltd., 2013.